0.1% Tween 20 and incubated with anti-rabbit or mouse-immunoglobulin G coupled to peroxidase (Amersham Bioscience, Buckinghamshire, UK) for 1 hr at room temperature. Reactive bands were detected using ECL chemiluminesence reagent (Amersham Bioscience). The specific bands were subjected to densitometery analysis by using the ImageJ program provided by the National Institutes of Health (Bethesda, MD).

Enzyme-linked immunosorbent assay

After 24-hr incubation, periostin levels in the culture supernatant were determined by the enzyme-linked immunosorbent assay (ELISA). Briefly, ELISA immunoassay plates (Becton Dickson, Franklin Lakes, NJ) were coated with the samples overnight at 4°C. After coating, the plates were incubated with 5% dry milk to block uncoated sites. After washes with phosphate-buffered saline, rabbit anti-periostin antibody (at 1:2000 dilution) was added and incubated for 1 hr at room temperature. After washes, goat anti-rabbit IgG antibody conjugated with horseradish peroxidase (Southern Biotechnology, Birmingham, AL) was added and incubated for 1 hr. After final washes, 3,3′,5,5′-tetramentylbenzidine (Pierce, Rockford, IL) was added. The periostin concentration was determined by differences in absorbance at wavelength 450 minus 550 nm. Recombinant periostin served as a standard control.

Fluorescent immunohistochemistry

Periostin- or EV-transfected Panc1 cells were grown to subconfluence on BD Falcon™ culture slides (BD Biosciences, San Jose, CA) and fixed with cold methanol (Wako, Osaka, Japan). After blocking with normal goat serum, the cells were incubated with mouse monoclonal E-cadherin antibody (BD Transduction Laboratories) and monoclonal mouse β-catenin antibody(BD Transduction Laboratories) overnight at 4°C and then the slides were incubated with fluorescein-conjugated goat anti-mouse IgG (Jackson ImmunoReserch laboratories, West Grove, CA). Cells were then incubated with propidium iodide (Wako) for nuclear staining and mounted with Vectashield (Vector Laboratory). For double staining for periostin and α-SMA, cells were fixed with cold methanol. After blocking with 3% bovine serum albumin in PBS, the cells were incubated with rabbit polyclonal anti-periostin antibody and mouse polyclonal α-SMA antibody overnight at 4°C and then the slides were incubated with Alexa Fluor 546 donkey anti-goat IgG (Molecular Probes) and Alexa Fluor 488 donkey anti-rabbit IgG (Molecular Probes, Eugene), respectively, and mounted with Vectashield (Vector Laboratory). Cells were visualized for immunofluorescence with a Confocal TIRF-C1 microscope (Nikon Intstech, Kawasaki, Japan).

Cell growth assays

Cell growth was assessed by direct count and 5-bromo-2-deoxyuridine (BrdU) assay. For the direct count, pancreatic cancer cells were grown in 6-well culture dishes (BD Falcon) with normal growth media. Cells were counted using a hemocytometer every day (days 1, 2, 3, 4 and 5) after removing the cells from the plates with 0.5 g/l trypsin. For BrdU assay, 6,000 periostin-transfected cells or EV cells were seeded per well in 96-well plates (BD Falcon) in normal cell growth media. The BrdU assay was performed after 24, 48 and 72 hr incubation using a kit (Roche) according to the manufacturer's protocol. For each cell line, the proliferation index was evaluated and absorbance at 48 and 72 hr was normalized to that at 24 hr.

Scrape motility assay

Pancreatic cancer cells were grown to confluency in 12-well culture dishes (BD Falcon) with normal growth media. The cell monolayer was mechanically scratched with a sterile pipette tip. Subsequently, the plates were incubated with serum-free DMEM including recombinant periostin (0 to 1 μg/ml) or the supernatant from periostin-expressing or control 293T cells for additional 2 to 4 days. Cells were visualized with an Olympus MODEL CK2 inverted microscope using a 10× objective. Images were captured in a time-lapse manner with an Olympus C2000 digital camera. The scratched area covered by migrated cells was measured in 3 independent wells and normalized to the initially scratched area using Scion Image Software (Scion Corporation).

Two-chamber migration assays

Cell invasion was determined by using a modified 2-chamber migration assay (pore size of 8 mm, BD Biosciences) according to the manufacturer's instructions. 2.5×10^4 cells were seeded in serum-free medium in the upper chamber and migration during 24 hr toward the lower chamber which contained 10% FBS as a chemoattractant was evaluated. Cells in the upper chamber were carefully removed using a cotton bud, and cells at the bottom of the membrane were fixed and stained with Diff-Quick (International Reagents, Kobe, Japan). Quantification was performed by counting the stained cells.

Soft agar assay

Forty thousand PP1 or Panc1.EV cells per well were suspended in 0.3% Bacto ™ agar (BD Falcon) supplemented with DMEM medium containing 10% fetal bovine serum and were layered over 1 ml of a 0.8% agar-medium base layer in 6-well plates. After 21 days, viable colonies were stained with nitroblue tetrazolium (Roche) and anchorage-independent growth was estimated by counting the number of stained colonies using a high power microscope.

Tumor growth in nude mice

Tumor formation *in vivo* was assessed in female athymic nude mice by subcutaneous injection of 2×10^6 cells each, suspended in 200 μl of sterile PBS. The tumor volume was measured every week after the first detection of visible tumor formation. Volume was determined by the equation $V = L \times W^2 \times 0.5$, where V is volume, L is length and W is width. The mice were sacrificed 7 weeks after injection and the histology was examined by H&E staining.

Orthotopic implantation

To assess metastasis formation, periostin and EV-transfected Panc1 cells (1×10^6 cells suspended in 50 μl) were injected into the pancreatic tail of female athymic nude mice. The mice were sacrificed 9 weeks after injection and tumor progression was confirmed. Histology was evaluated by H&E staining.

Statistical analysis

Statistical analysis was performed and graphs were made with GraphPad Prism software (GraphPad Software, San Diego, USA). The correlation of periostin expression with the patients' clinicopathological variables and the correlation between periostin expression and frequency of metastasis in the orthotopically injected mice were analyzed by χ^2 test. The difference between 2 groups was analyzed by unpaired t test or Mann–Whitney U test. The p value <0.05 was regarded as statistically significant.

Results

Periostin expression and localization in pancreatic tissue and pancreatic cell lines

To evaluate the expression of periostin in the pancreatic tissues, immunostaining was performed in 61 human pancreatic tissues (2 normal pancreatic tissue, 32 pancreatic cancer, 13 intraductal papillary mucinous neoplasms and 10 chronic pancreatitis) and 4 cases of colonic cancer. The expression of periostin was not detected in pancreatic caricinoma cells, normal pancreatic ductal cells or colonic carcinoma cells. However, there was strong expression in the stromal cells adjacent to the epithelial cells in pancreatic and colonic tissues (Figs. 1*a*–1*d*, Table I). Since strong immunoreactivity was present in the stroma of pancreatic and

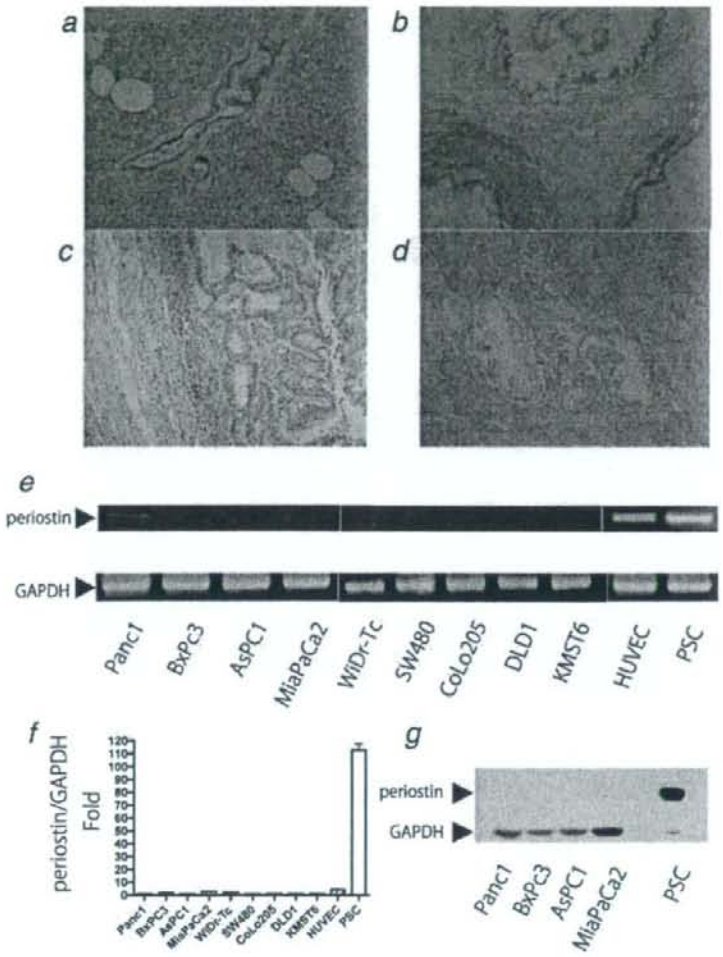

FIGURE 1 – Periostin expression in normal tissue of pancreas (*a*), IPMN (*b*), pancreatic cancer (*c*) and colonic cancer (*d*). *a*, Normal pancreatic duct and acinar cells showed no staining for periostin. *b–d*, Stromal areas of the sections showed positive staining for periostin, but tumor lesions showed no staining for periostin. *e–g*, Periostin expression in pancreatic cancer cell lines, colonic cancer cell lines and normal cultured cells (HUVEC, PSC). Periostin expression in cultured cells was examined by RT-PCR (*e*), quantitative real-time RT-PCR (*f*) and Western blot analysis (*g*). The expression of periostin mRNA was detected in PSC and in HUVEC while no or little expression was observed in carcinoma cell lines or KMST6 (fibroblastic cells). *f*, Expression of periostin mRNA was normalized to that of GAPDH mRNA. Values are expressed relative to 1.00 for expression in Panc-1 cells. Real-time RT-PCR clearly indicates the difference in the expression levels of periostin between pancreatic cancer cell lines and normal cultured cells. The highest expression was seen in PSC. *g*, Western blot analysis clearly showed that the expression of periostin protein is detected in PSC but not in pancreatic cancer cell lines.

TABLE I – THE ASSOCIATION OF THE EXPRESSION OF PERIOSTIN WITH EPITHELIAL DUCT OR STROMAL CELLS

	Cancer	Stroma	*p*-value
Pancreatic cancer ($n = 32$)	2/32	30/32	$p < 0.05$
IPMN ($n = 13$)	2/13	13/13	
Chronic pancreatitis ($n = 10$)	0/10	10/10	
Colonic cancer ($n = 4$)	0/4	4/4	

For the evaluation of the periostin expression, chi square test and fisher exact test were performed.

colonic carcinoma tissues, we investigated the expression of periostin by RT-PCR in cultured cell lines of various origin to elucidate the source of this gene. The cultured cell lines we used were primary cultures of human PSCs, cultured pancreatic cancer cells (Panc1, AsPC1, MiaPaCa2, BxPC3), cultured colonic cancer cells (WiDr-Tc, SW480, CoLo205, DLD1), cultured human fibroblasts (KMST6) and HUVEC. Among these cell lines, the expression of periostin mRNA was detected in HUVEC and PSC while little or no expression of this gene was found in pancreatic and colonic cancer cell lines (Fig. 1*e*). The quantitative real-time RT-PCR

showed a difference in the periostin expression level and revealed higher expression in normal cultured cells (PSC or HUVEC) than in carcinoma cells (Fig. 1*f*). Western blot analysis also revealed that the expression of periostin protein was detected only in PSC but not in pancreatic cancer cell lines (Fig. 1*g*).

Periostin expression was increased in peritumoral stroma

To determine the source of periostin in human pancreatic cancer tissues, double immunofluorescence immnohistochemistry was performed using periostin and α-SMA antibodies on frozen tissue sections. As shown in Figure 2*a*, stromal cells adjacent to carcinoma cells coexpressed periostin and α-SMA, suggesting that periostin was localized in mesenchymal cells. To compare the intensity of gene expression between the carcinoma lesion and stromal area, the ductal adenocarcinoma lesion and stromal area were carefully microdissected and were subjected to quantitative real-time RT-PCR (Fig. 2*b*). As shown in Figure 2*b* (b and c), stromal cells expressed significantly higher level of periostin than did cancer cells. These findings indicate that stromal cells but not carcinoma cells are a source of periostin in human pancreatic cancer tissues.

Periostin plays an important role in epithelial mesenchmal interaction

Because periostin is a secretory protein that was found abundantly in the stromal area as described earlier, we analyzed the effect of secreted periostin on pancreatic cancer cells. We established 293T cells transiently expressing periostin and collected the supernatant where periostin expression was clearly detected (Fig. 3*a*). Using this supernatant, we examined the cell migration ability of Panc1 cells by wound healing scratch assay. As shown in Figure 3*b*, Panc1 cells with the supernatant from 293T-peri cells did not cover the scratched area with migrating cells while those with the supernatant from control 293T cells showed many cells in the scratched area, indicating that secreted periostin inhibits the cell migration of pancreatic cancer cells. Taken together with the results that stromal cells but not cancer cells were the source of periostin, we hypothesized that secreted periostin from stromal cells inhibits the migration of pancreatic cancer cells. Therefore, we next investigated whether pancreatic cancer cells had an effect on stromal cells in cocultured system. Panc1 and rat PSC cells were cocultured in a contact condition, as described in Material and Methods, and the expression level of rat-periostin was determined after 24 hr of incubation by real-time RT-PCR analysis using specific primers for rat periostin that did not recognize human periostin (Fig. 3*c*). As shown in Figure 3*d*, the significant induction of periostin mRNA that originated from PSC was observed only when PSC was cocultured with Panc1, suggesting that pancreatic cancer cells could induce the expression of periostin in PSC.

To confirm the interaction between carcinoma cells and stromal cells *in vivo*, pancreatic cancer cells (BxPC3) were subcutaneously injected into nude mice with periostin overexpressing (KMSTp18) or control fibroblastic cell lines with EV (KMST6). In all animals, pancreatic carcinoma cells with control fibroblastic cells grew faster than those with periostin expressing fibroblastic cells. In addition, BxPC3 coinjected with KMST6 showed significantly larger tumors compared with BxPC3 coinjected with KMSTp18 (Fig. 3*e*). These findings suggested that secreted periostin from stromal cells inhibit pancreatic cancer cell growth *in vivo*.

Generation of stable periostin-expressing cell line

Since secreted periostin suppressed the migration or growth of pancreatic cancer cells *in vitro* and *in vivo*, we postulated that this gene functions as a tumor suppressor in pancreatic carcinoma cells. Therefore, we generated stably expressing pancreatic cancer cells. Panc1 cells were transfected with periostin expression vector and were cloned, and the expression of this gene was confirmed by quantitative real-time RT-PCR and Western blot. Among several clones expressing periostin mRNA, we confirmed one clone (PP1) which also expressed periostin protein (Figs. 4*a*–4*c*). A morphological difference was observed between control (parental and EV transfected Panc1) and priostin expressing Panc1 cells (PP1). Control cells fundamentally showed loose cell attachment and scattered morphology like mesenchymal cells, while PP1 demonstrated cobblestone-like appearance (Fig. 4*d*).

Expression of periostin-induced epithelial characteristics

To investigate whether the enhanced expression of periostin would affect epithelial and mesenchymal markers in cultured tumor cells *in vitro*, we performed immunofluorescence staining and western blot analysis for epithelial and mesenchymal markers on periostin- or EV-transfected Panc1 cells. As shown in Figure 3*e*, PP1 cells showed dominant membrane-bound staining of E-cadherin and β-catenin while control cells (Panc1.EV) exhibited a weak and diffuse distribution of epithelial markers. In contrast, the expression of mesenchymal markers (vimentin and N-cadherin) was reduced in PP1 cells compared with control cells (Panc1.EV). Consistent with these findings, western blot analysis also showed increased expression of epithelial markers (β-catenin, E-cadherin) and decreased expression of mesenchymal markers (N-cadherin, Vimentin). These molecular changes implied that the induced expression of periostin shifted the Panc1 cells from the mesenchymal to epithelial phenotype.

Expression of periostin results in interference with cell migration, and spread in vitro

To assess the effects of periostin on pancreatic cancer proliferation, cell count assay (Fig. 5*a*) and BrdU incorporation assay (Fig. 5) were performed. Neither of these analyses showed significant differences in cell proliferation between controls and periostin-expressing cells. To elucidate the function of periostin in the anchorage-independent growth of pancreatic cancer cells, we utilized the soft agar assay. PP1 and control cells showed similar numbers of colonies on soft agar (Fig. 5*c*).

We next examined the cell migration ability of PP1 cells by wound healing scratch assay. As shown in Figure 5*d*, Panc1.EV cells covered the scratched area with migrating cells within 48 hr but periostin expressing cells did not. The 2-chamber migration assays also revealed significantly fewer PP1 cells migrating to the lower chamber compared with the control cells (Fig. 5*e*).

To determine the activation of the Akt signaling pathway in the periostin-overexpressing and control cells, we employed western blot using a specific antibody for phosphorylated Akt. Interestingly, the phosphorylation of AKT was not observed in periostin-overexpressing cells whereas it was weakly observed in control cells (Fig. 5*f*).

Periostin has biphasic effects on the migration of pancreatic cancer cells

Because these tumor suppressive effects of periostion were inconsistent with previous studies in pancreatic cancer, we considered that the effect of periostin on the biological aggressiveness of pancreatic cancer may depend on the concentration of this protein. Therefore, we measured the concentration of periostin in the supernatant of cell lines by ELISA. The concentration of supernatants from 293T-peri cells, PP1 cells and PSC cells was approximately 150 ng/ml (Fig. 6*a*). We then examined whether the differences of the periostin concentrations affected the cell migration of Panc1 cells. As shown in Figure 6*b*, periostin at 100 ng/ml of concentration suppressed migration of Panc1 as assessed by wound healing scratch assay. In contrast, 1 μg/ml of periostin induced migration of Panc1. To elucidate the mechanism of the induction of the cell migration, the downstream signaling pathways of periostin were investigated. We treated Panc1 cells with 100 ng/ml or 1 μg/ml of periostin and assessed Akt phosphorylation by Western blotting. The phosphorylation of Akt was clearly induced when Panc1 was treated with 1 μg/ml of periostin (Fig. 6*c*, right panel),

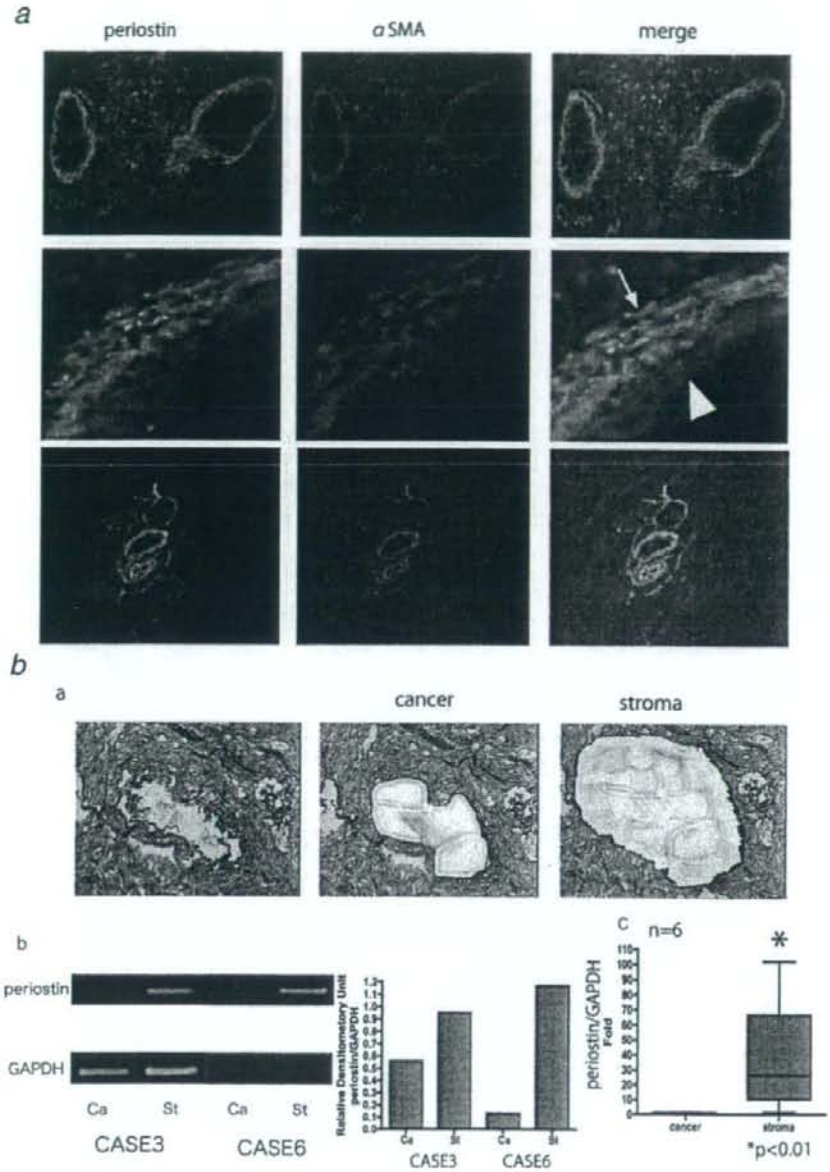

FIGURE 2 – The expression of periostin was found in stromal cells but not carcinoma cells. *a*, Double immunofluorescence staining reveals co-localization of periostin and αSMA in the pericyte and stromal area in human pancreatic cancer tissues. Periostin and αSMA expression was observed in tumor pericyte (arrow in middle panel) and stromal cells but not or background level in tumor cells (arrow head in middle panel). Coexpression of periostin and αSMA in stromal cells was frequently seen adjacent carcinoma cells (upper panel) while stromal cells around vessel infrequently demonstrated simultaneous expression these proteins (lower panel). Vessel cells showed intense coexpression of periostin and αSMA. *b*, RNA expression of periostin in microdissected cancer and stromal lesions in the pancreatic cancer. Total RNA was extracted from the microdissected lesions. Toluidine blue-stained carcinoma and stromal lesions were cut by a laser and recovered in lysis buffer (a). The real-time RT-PCR analysis clearly showed stronger expression of periostin in stromal cells than in carcinoma cells (b and c). Each sample's periostin expression level was normalized by the corresponding GAPDH expression level.

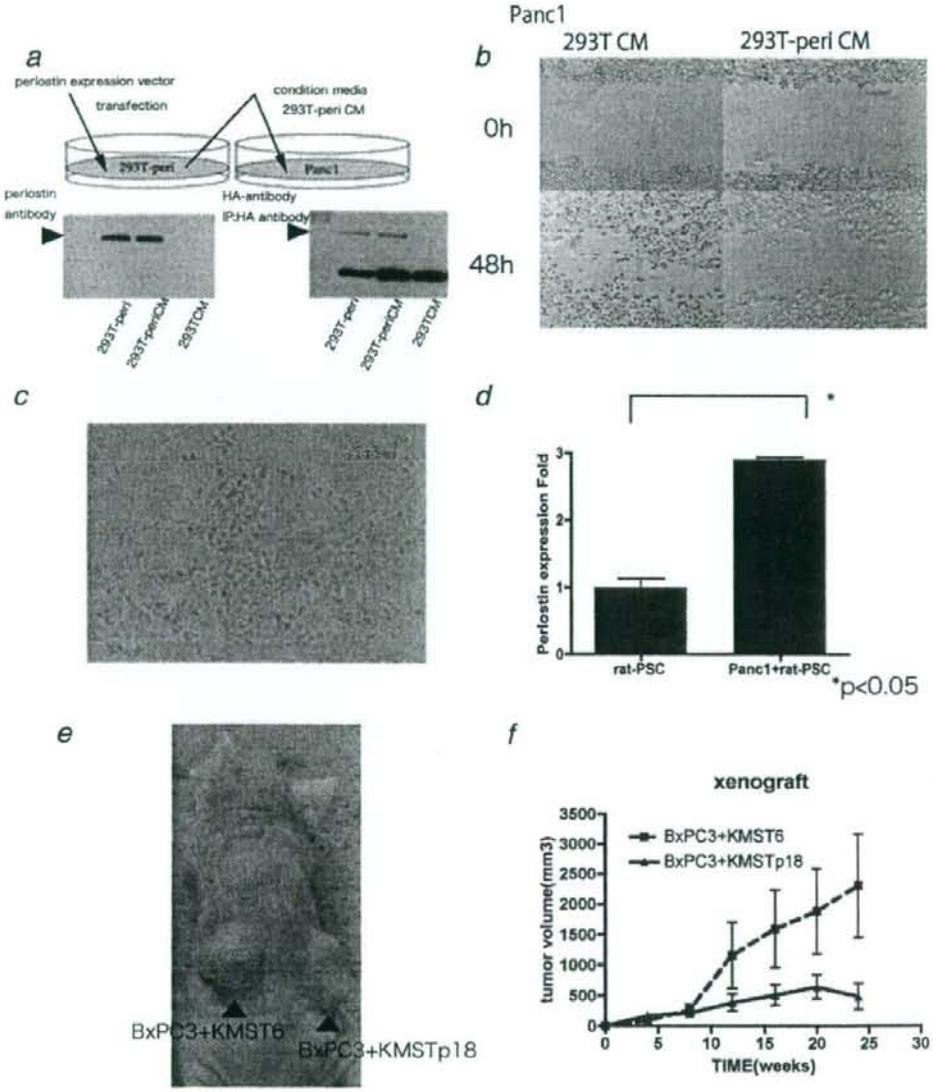

FIGURE 3 – Secreted periostin from stromal cells inhibited pancreatic cancer cell migration and tumor formation in nude mice. *a*, We established periostin expressing 293T cells (293T-peri) and collected the supernatant. Cell lysate from 293T-peri cells and the supernatant from these cells were immunoprecipitated with anti HA antibody and then western blot analyses were performed using periostin (lower left panel) and HA (lower right panel) antibody. *b*, The wound healing scratch assay of Panc1 with or without the supernatant from periostin expressing 293T cells. There were many migrated cells in the cell space after 48 hr culture with the conditioned media from control 293T, while few cells were observed in the space when Panc1 cells were cultured with media from 293-peri. *c*, Panc1 cells and rat-PSC were cocultured in contact conditions. Panc1 cells were added to monolayer of rat-PSC. Total RNA was extracted after 24 hr incubation and was subjected to real-time RT-PCR to evaluate periostin expression. The expression of periostin mRNA in the rat-PSC was significantly induced when these cells were cocultured with Panc-1 cells (*d*). *e*, BxPC3 cells together with KMST6 cells and those with periostin-overexpressing KMST6 cells (KMSTp18) were injected into the left side and the right side of the same nude mice, respectively (left panel). The tumor volume was calculated by using formula ($V = L \times W^2 \times 0.5$ (V is volume, L is length and W is width)). After 9 weeks, the mice were sacrificed. BxPC3 cells with periostin-overexpressing KMST6 cells (KMSTp18) exhibited slower growth as well as smaller tumor size in nude mice relative to those with control cells (right graph). *$p < 0.01$.

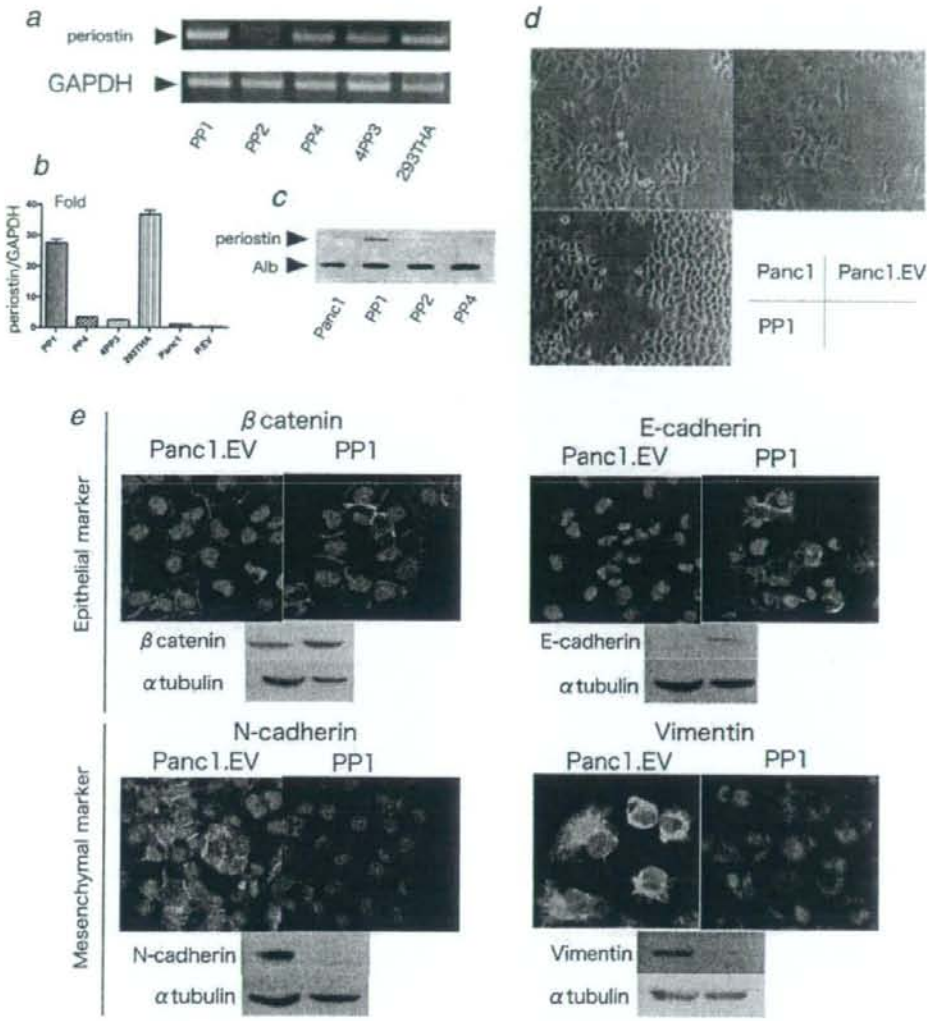

FIGURE 4 – Induced expression of periostin resulted in reversal of EMT in pancreatic cancer cells. *a*: RT-PCR analysis of periositn mRNA in several clones of periostin expression vector-transfected Panc1 and 293T cells. Specific bands for periostin were observed in all transfected cells except the PP2 clone. *b*, Real-time quantitative RT-PCR analysis of periostin mRNA level in several periostin transfected Panc1 cells and 293T cells. *c*, Forced periostin protein expression is confirmed by immunoprecipitation and Western blot analysis using anti HA antibody. *d*, Phase-contrast photographs of the Panc1 series. Panc1 and Panc1.EV cells exhibit fibroblastoid morphology, whereas PP1 cells exhibit a cuboidal epithelial morphology. *e*, Immunofluorescent staining for epithelial markers (E-cadherin and β-catenin) and mesenchymal markers (vimentin and N-cadherin) was performed in empty vector or periostin-transfected Panc1 cells. The panels under the immunofluorescent staining showed the results of Western blot analysis using the same antibody as in the upper panel and α-tubulin as loading control. Both methods clearly demonstrated that the epithelial markers were down-regulated in Panc1.EV cells but up-regulated in PP1cells. Commensurately, the mesenchymal markers were up-regulated in Panc1.EV cells, but they were down-regulated in PP1 cells.

while its phosphorylation was reduced by the treatment with 100 ng/ml of periostin compared to basal level (Fig. 6*c*, left panel). These observations clearly indicated the biphasic effect that the low concentration inhibited and the high concentration accelerated the migration of pancreatic carcinoma cells, at least in part, through the regulation of the activation of AKT.

Periostin inhibits cell growth and metastasis in nude mice

To assess whether periostin suppresses tumor growth *in vivo*, 2×10^6 of EV cells or PP1 cells were injected subcutaneously into the dorsal flank of nude mice. The tumors arising from periostin expressing cells showed significantly slower growth and were smaller compared with those of Panc1.EV (Fig. 7*a*).

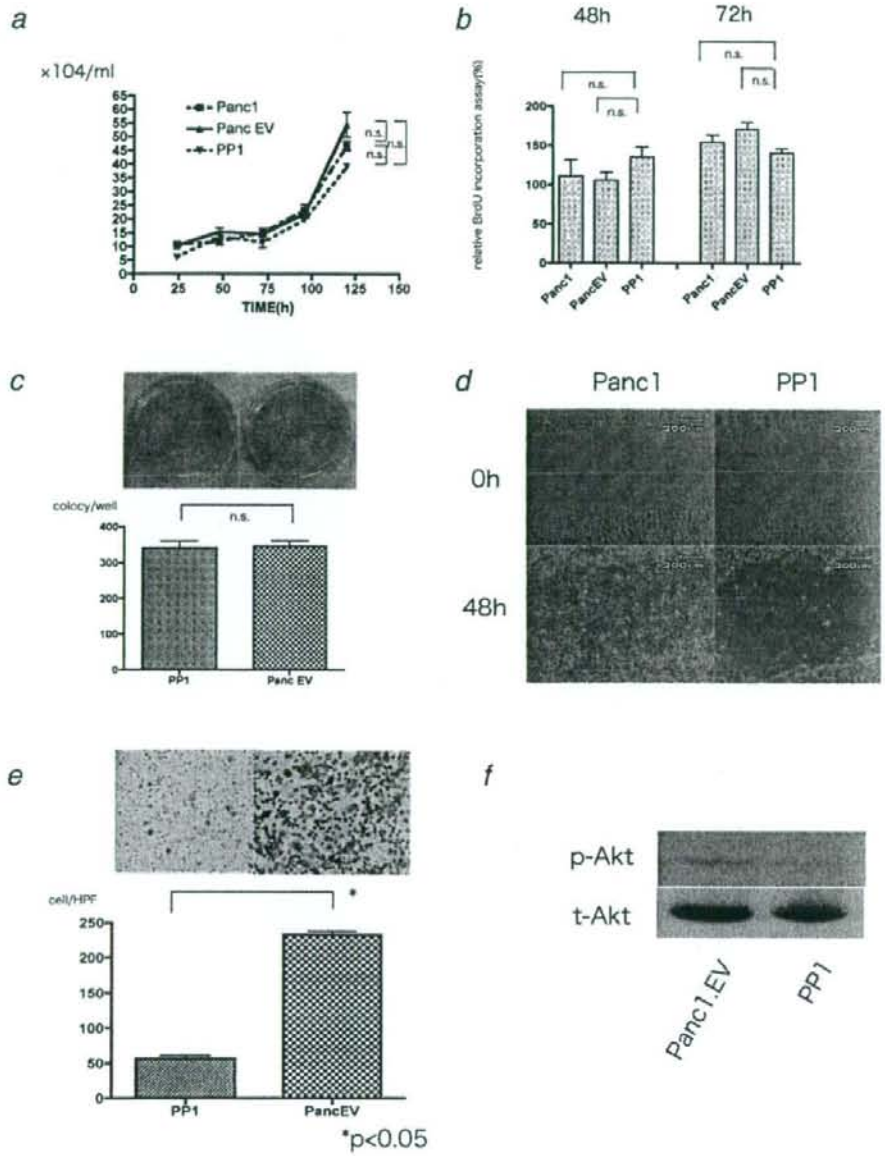

FIGURE 5 – Periostin reduced the pancreatic cancer cell migration. *a*, Panc1 and PP1 cells were seeded in a 6-well plate with normal growth media. After 1, 2, 3, 4 and 5 days, cell numbers were counted using a hemocytometer. No significant difference was observed in these cells. *b*, Panc1 and PP1 cells were seeded in 96-well plates. BrdU assay was performed after 24, 48 and 72 hr incubation using a kit according to the manufacturer's protocol. For each cell line the Proliferation Index was evaluated and the absorbance at 48 and 72 hr normalized to that at 24 hr. *c*, Equal numbers of Panc1 cells either with the periostin expressing vector (PP1) or with the control vector (Panc1.EV) were grown in soft agarose for 3 weeks. *d*, Periostin-overexpressing cells showed significantly slower migration compared with Panc1.EV. The scratched area covered by migrated cells was measured in 3 independent wells. Periostin expressing cells showed fewer migrated cells than control cells did. *e*, 2.5×10^4 Panc1 cells transfected with empty vector or periostin expression vector were seeded into upper chamber in serum free condition and cells that migrated toward the lower chamber, filled with media with 10% FBS as a chemoattractant, were counted after 24 hr. PancEV cells showed greater migration to the lower chamber compared to PP1 cells. *f*, Immunoblot analysis of Akt phosphorylation. The level of phosphorylated Akt was decreased in periostin-transfected cells as compared with control Panc1 cells.

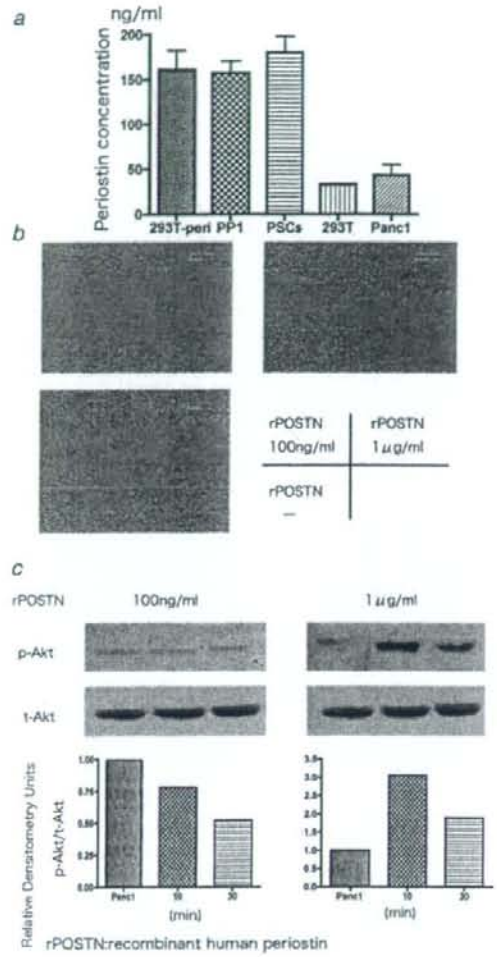

FIGURE 6 – The effects of periostin on migration are dependent on its concentration. *a*, After 24-hr incubation, periostin levels in the culture supernatant were determined by ELISA. Data shown are expressed as means + SD ($n = 3$). *b*, The wound healing scratch assay after 48 hr incubation with the various concentration of periostin (0 to 1 μg/ml). There were many migrated cells in the cell space after 48 hr culture with 1 μg/ml of human periostin, while few cells were observed in the space when Panc1 cells were cultured with 100 ng/ml of human periostin. In addition, the pancreatic carcinoma cells treated with 100 ng/ml showed fewer migrated cells in the cell space than control cells did. *c*, Western blot analyses revealed that phosphorylation of AKT was induced when Panc-1 cells were treated with 1 μg/ml of periostin (right panel) and was reduced by the treatment with 100 ng/ml of periostin. The bar graph clearly showed the reduction and induction of AKT phosphorylation by incubation with low concentration (100 ng/ml) and high concentration (1 μg/ml) of periostin, respectively.

To further evaluate if periostin overexpression affects metastasis *in vivo*, we implanted the PP1 cells and control cells (Panc1.EV) by injecting them orthotopically into the pancreatic tail of nude mice. Nine weeks after the injection, mice were sacrificed. Tumors

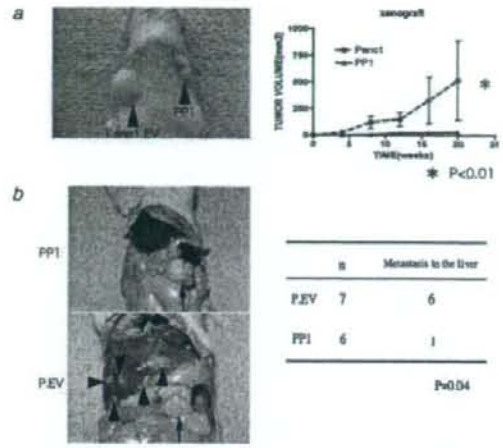

FIGURE 7 – Periostin significantly suppressed the tumor formation and the metastasis to the liver in nude mice. *a*, Two million control (Panc1.EV) cells or periostin-expressing (PP1) cells were injected subcutaneously into the left and right side of each mouse, respectively. The tumor volume was calculated by using the formula ($V = L \times W^2 \times 0.5$ (V is volume, L is length, and W is width)). After 9 weeks, the mice were sacrificed. PP1 cells exhibited slower growth as well as smaller tumor size in nude mice compared with Panc1.EV cells. $*p < 0.01$. *b*, Expression of periostin reduced metastasis of pancreatic carcinoma cells in orthotopic implantation in nude mice. Panc1.EV and PP1 cells were injected into the pancreatic tail of nude mice to examine whether the expression of periostin suppresses pancreatic cancer cell development. Seven of 7 mice with control cells and 6 of 7 mice with PP1 cells showed tumors in the pancreatic tail (arrow in B, upper panel) 9 weeks after orthotopic implantation, respectively. Six of 7 mice implanted with control cells demonstrated metastasis to the liver (arrow head in B, left lower panel), while only 1 of 6 mice implanted with PP1 cells showed metastasis to the liver.

were observed in the pancreata of both of the mice implanted with periostin-expressing cells and those with control cells. Interestingly, the periostin-expressing cells did not metastasize to the liver while multiple metastases to the liver were found in mice implanted with control cells. These findings suggested that periostin could inhibit metastasis to distant organs (Fig. 7*b*).

Discussion

Periostin contains an N-terminal secretory signal peptide, followed by a cysteine-rich domain, 4 internal homologous repeats and a C-terminal hydrophilic domain. Periostin from osteoblasts was originally identified to function as a cell adhesion molecule for preosteoblasts and precipitate in osteoblast recruitment, attachment and spreading.[16,17] Recently, proteomic and microarray profiling studies showed that periostin is up-regulated in pancreatic cancer tissues.[18–20] However, it has been demonstrated that periostin protein was mainly detected in the juxtatumoral stroma components, while the tumor cells themselves showed no immunoreactivity. Consistently, quantitative real-time RT-PCR revealed that periostin was not or very faintly expressed in pancreatic cancer cell lines, but it was strongly expressed in PSC.[12,13] In agreement with these findings, we also showed much higher levels of both periostin mRNA and protein in stromal lesions compared with those in cancer cells. In addition, PSC expressed larger amounts of periostin than cancer cells did. From these findings, we conclude that stromal cells are the major source of periostin in human pancreatic cancer tissues.

For most carcinoma, progression toward malignancy is accompanied by a loss of epithelial differentiation and a shift toward a mesenchymal phenotype. This process, referred to as "epithelial to mesenchymal transition (EMT)," intensifies the motility and invasiveness of many cell types and is often considered a prerequisite for tumor infiltration and metastasis.[3,4] Pancreatic cancer is the fourth leading cause of cancer-related deaths in the industrialized world.[21] Once pancreatic cancer is clinically evident, it rapidly develops metastatic lesions, frequently by the time of diagnosis. In addition, these tumors are usually resistant to chemotherapy and radiation.[22,23] Therefore, a new therapeutic strategy is required to improve the prognosis. We previously showed that Bone Morphogenetic Protein 4 (BMP4) induced EMT in pancreatic cancer cells with up-regulation of MSX2, and inactivation of MSX2 by siRNA suppressed EMT and inhibited the growth and metastasis of pancreatic cancer *in vivo*, suggesting that blockade of EMT could suppress tumor development. Therefore, EMT could be a candidate for a new therapeutic approach.[24,25] In the current study, induction of periostin expression to a lesser extent in pancreatic cancer cells also resulted in a reversal of the state of EMT and reduced the metastatic potential *in vivo*. Since periostin has biphasic effect, it might be one of the key genes to regulate EMT depending on the status of microenvironment.

Previous studies showed that periostin was up-regulated in various types of cancers such as the lung,[26] brain,[8] ovary,[9] breast,[27] colon[11] and oral cavity,[28,29] and its serum level was reported to be high in patients with thymoma,[30] non-small cell lung cancer[10] and breast cancer.[31] These reports suggested that periostin is involved in tumor spread, invasion and metastasis. At the molecular level, periostin activated the Akt/PKB signaling pathway[11] through $\alpha v\beta 3$[9] or $\beta 4$[12] integrins to increase cell survival. These results were entirely opposite to our findings. Erkan *et al.* have reported that periostin had biphasic effects on the Akt phosphorylation of pancreatic cancer cells. They have shown that periostin significantly decreased the Akt phosphorylation at a dose of 100 ng/ml while it increased its phosphorylation at 1 μg/ml.[13] Therefore, the present results of periostin's suppressive effects on malignant behavior of pancreatic cancer cells may have been caused by its low concentrations in the supernatants of 293T-peri cells and PP1 cells. In fact, the concentration of periostin in the supernatants from these cells was approximately 150 ng/ml which was 1/7 lower than that was used in previous study. Consistently, periostin was reported to suppress the invasiveness and metastasis of various carcinoma cells, suggesting that periostin was a tumor suppressor.[32,33] In addition, Hartel, *et al.* demonstrated that connective tissue growth factor (CTGF) was expressed dominantly in the stromal area in pancreatic cancer tissues and that patients showing high CTGF mRNA expression levels had better prognoses, indicating that desmoplastic reaction, a prominent stromal/fibrous reaction in and around tumor tissues observed in most pancreatic cancer, provides a growth disadvantage for pancreatic cancer cells.[34] This finding also supports the tumor suppressive effect of periostin because periostin was shown to be the down stream target of CTGF.[35] Although the discrepant effect of periostin for various tumors' development may be explained by its biphasic effect, it is not clear whether the desmoplastic reaction is a defense mechanism against cancer cell spreading or a growth advantage for pancreatic cancer cells.[34,36,37] Since periostin was abundantly secreted from PSC, which play a pivotal role in desmoplastic reaction,[36] and periostin has biphasic function to gain or decrease tumor aggressiveness, desmoplastic reaction may work as tumor promoter as well as tumor suppressor according to the expression level of periostin. Further study will be required to clarify the role of desmoplastic reaction and relation with periostin in pancreatic carcinoma development.

In conclusion, we demonstrated that stromal cells are the source of periostin in pancreatic cancer tissues. Pancreatic cancer cells stimulate stromal cells to secrete periostin, suggesting that cross talk between cancer cells and mesenchymal cells might further increase the periostin production in the desmoplasia. Finally, we have shown that overexpression of periostin to a lesser extent resulted in the mitigation of EMT and suppressed tumor cell metastasis, and that high concentration of periostin promoted the cell migration. These findings suggested that periostin is one of the key factors to regulate tumor-stromal interaction to accelerate or reduce tumor activity.

Acknowledgement

We thank Dr. Inoue for the periostin cDNA vector.

References

1. Hay E. An overview of epithelio-mesenchymal transformation. Acta Anat (Basel) 1995;154:8–20.
2. Thiery JP. Epithelial–mesenchymal transitions in development and pathologies. Curr Opin Cell Biol 2003;15:740–6.
3. Thiery JP. Epithelial–mesenchymal transitions in tumour progression. Nat Rev Cancer 2002;2:442–54.
4. Petersen OW, Nielsen HL, Gudjonsson T, Villadsen R, Rank F, Niebuhr E, Bissell MJ, Ronnov-Jessen L. Epithelial to mesenchymal transition in human breast cancer can provide a nonmalignant stroma. Am J Pathol 2003;162:391–402.
5. Christiansen JJ, Rajasekaran AK. Reassessing epithelial to mesenchymal transition as a prerequisite for carcinoma invasion and metastasis. Cancer Res 2006;66:8319–26.
6. Takeshita S, Kikuno R, Tezuka K, Amann E. Osteoblast-specific factor 2: cloning of putative bone adhesion protein with homology woth the insect protein fasciclin I. Biochem J 1993;294:271–8.
7. Horiuchi K, Amizuka N, Takeshita S, Takamatsu H, Katsuura M, Ozawa H, Toyama Y, Bonewald LF, Kudo A. Identification and characterization of a novel protein, periostin, with restricted expression to periosteum and periodontal ligament and increased expression by transforming growth factor beta. J Bone Miner Res 1999;14:1239–49.
8. Sasaki H, Sato Y, Kondo S, Fukai I, Kiriyama M, Yamakawa Y, Fuji Y. Expression of the periostin mRNA level in neuroblastoma. J Pediatr Surg 2002;37:1293–7.
9. Gillan L, Matei D, Fishman DA, Gerbin CS, Karlan BY, Chang DD. Periostin secreted by epithelial ovarian carcinoma is a ligand for alpha(V)beta(3) and alpha(V)beta(5) integrins and promotes cell motility. Cancer Res 2002;62:5358–64.
10. Sasaki H, Lo KM, Chen LB, Auclair D, Nakashima Y, Moriyama S, Fukai I, Tam C, Loda M, Fujii Y. Expression of Periostin, homologous with an insect cell adhesion molecule, as a prognostic marker in non-small cell lung cancers. Jpn J Cancer Res 2001;92:869–73.
11. Bao S, Ouyang G, Bai X, Huang Z, Ma C, Liu M, Shao R, Anderson RM, Rich JN, Wang XF. Periostin potently promotes metastatic growth of colon cancer by augmenting cell survival via the Akt/PKB pathway. Cancer Cell 2004;5:329–39.
12. Baril P, Gangeswaran R, Mahon PC, Caulee K, Kocher HM, Harada T, Zhu M, Kalthoff H, Crnogorac-Jurcevic T, Lemoine NR. Periostin promotes invasiveness and resistance of pancreatic cancer cells to hypoxia-induced cell death: role of the beta4 integrin and the PI3k pathway. Oncogene 2007;26:2082–94.
13. Erkan M, Kleeff J, Gorbachevski A, Reiser C, Mitkus T, Esposito I, Giese T, Buchler MW, Giese NA, Friess H. Periostin creates a tumor-supportive microenvironment in the pancreas by sustaining fibrogenic stellate cell activity. Gastroenterology 2007;132:1447–64.
14. Bachem MG, Schneider E, Gross H, Weidenbach H, Schmid RM, Menke A, Siech M, Beger H, Grunert A, Adler G. Identification, culture, and characterization of pancreatic stellate cells in rats and humans. Gastroenterology 1998;115:421–32.
15. Masamune A, Satoh M, Kikuta K, Suzuki N, Shimosegawa T. Establishment and characterization of a rat pancreatic stellate cell line by spontaneous immortalization. World J Gastroenterol 2003;9:2751–8.
16. Skonier J, Neubauer M, Madisen L, Bennett K, Plowman GD, Purchio AF. cDNA cloning and sequence analysis of beta ig-h3, a novel gene induced in a human adenocarcinoma cell line after treatment with transforming growth factor-beta. DNA Cell Biol 1992;11:511–22.
17. LeBaron RG, Bezverkov KI, Zimber MP, Pavelec R, Skonier J, Purchio AF. Beta IG-H3, a novel secretory protein inducible by transforming growth factor-beta, is present in normal skin and promotes the adhesion and spreading of dermal fibroblasts in vitro. J Invest Dermatol 1995;104:844–9.

The American Journal of Pathology, Vol. 172, No. 4, April 2008

DOI: 10.2353/ajpath.2008.070346

Gastrointestinal, Hepatobiliary and Pancreatic Pathology

Up-Regulation of MSX2 Enhances the Malignant Phenotype and Is Associated with Twist 1 Expression in Human Pancreatic Cancer Cells

Kennichi Satoh,* Shin Hamada,* Kenji Kimura,* Atsushi Kanno,* Morihisa Hirota,* Jun Umino,* Wataru Fujibuchi,† Atsushi Masamune,* Naoki Tanaka,‡ Koh Miura,‡ Shinichi Egawa,‡ Fuyuhiko Motoi,‡ Michiaki Unno,‡ Barbara K. Vonderhaar,§ and Tooru Shimosegawa*

From the Division of Gastroenterology, and the Department of Gastroenterological Surgery,‡ Tohoku University Graduate School of Medicine, Sendai City, Miyagi, Japan; Advanced Industrial Science and Technology,† Koto-ku, Tokyo, Japan; and the Mammary Biology and Tumorigenesis Laboratory,§ National Cancer Institute, National Institutes of Health, Bethesda, Maryland

MSX2 is thought to be a regulator of organ development and a downstream target of the *ras* signaling pathway; however, little is known about the role of MSX2 in the development of pancreatic cancers, most of which harbor a K-*ras* gene mutation. Therefore, we examined whether the presence of MSX2 correlates with the malignant behavior of pancreatic cancer cells. BxPC3 pancreatic cancer cells that stably overexpress MSX2 showed a flattened and scattered morphology accompanied by a change in localization of E-cadherin and β-catenin from membrane to cytoplasm. Cell proliferation rate, cell migration, and anchorage-independent cell growth were enhanced in MSX2-expressing cells. Injection of MSX2-expressing cells into the pancreas of nude mice resulted in a significant increase in liver metastases and peritoneal disseminations compared with injection of control cells. Microarray analysis revealed a significant induction of Twist 1 expression in cells that express MSX2. When MSX2 was inactivated in pancreatic cancer cells following transfection with an MSX2-specific small interfering RNA, Twist 1 was down-regulated. Immunohistochemistry of human pancreatic carcinoma tissue revealed that MSX2 was frequently expressed in cancer cells, and that increased expression of MSX2 significantly correlated with higher tumor grade, vascular invasion, and Twist 1 expression. These data indicate that MSX2 plays a crucial role in pancreatic cancer development by inducing changes consistent with epithelial to mesenchymal transition through enhanced expression of Twist 1. *(Am J Pathol 2008, 172:926–939; DOI: 10.2353/ajpath.2008.070346)*

Homeobox-containing genes have been shown to be major regulators of morphological development of a variety of organs, and their expression levels vary during different stages of organ development.[1,2] Msx2, a member of the homeobox genes (Hox gene) family, is present in a variety of sites, including premigratory cranial neural crest, tooth, retina and lens, apical ectodermal ridge, and mammary gland.[3–9] In the development of these organs, the expression patterns of this gene suggests its active involvement in epithelial-mesenchymal interactions.

On the other hand, enhanced levels of transcripts for MSX2, the human homologue of Msx2 (HOX-8), have been shown in a variety of carcinoma cell lines of epithelial origin compared to their corresponding normal tissues. However, this enhanced expression is not found in hematopoietic tumor cells, suggesting that MSX2 plays a more important role in tumors of epithelial origin than in those of hematopoietic origin.[10] Expression of endogenous MSX2 also is up-regulated in v-Ki-*ras*-transfected NIH3T3 cells.[11] Although MSX2 itself failed to confer a transformed phenotype, antisense MSX2 cDNA as well as truncated MSX2 cDNA interfered with the transforming activities of both the v-K-*ras* and v-*raf* oncogene.[11] These findings indicated that MSX2 might be an important downstream target for the *Ras* signaling pathway. In addition, MSX2 activates cyclin D1 expression and inhibits cellular

Supported in part by grants-in-aid 17390213 and 19590745 from the Ministry of Education, Science, Sports and Culture of Japan.

Accepted for publication January 15, 2008.

Supplemental material for this article can be found on *http://ajp.amjpathol.org*.

Address reprint requests to Kennichi Satoh, Division of Gastroenterology, Tohoku University Graduate School of Medicine, 1-1, Siryo-machi, Aobaku, Sendai City, Miyagi, 980-8574, Japan. E-mail: ksatoh@mail.tains.tohoku.ac.jp.

differentiation as shown in the mouse myogenic cell line C2C12,[12] suggesting a relation of MSX2 with tumorigenesis since cyclin D1 overexpression is found in various carcinomas such as breast[13,14] and pancreatic cancer.[15]

Pancreatic cancer is one of the most malignant gastrointestinal tumors. Once pancreatic cancer is clinically evident, it progresses rapidly to develop metastatic lesions, frequently by the time of diagnosis. Furthermore, these tumors are usually resistant to conventional chemotherapy and radiation therapy. The pathogenic mechanisms that regulate the aggressive behavior of this cancer still remain to be clarified. Although most pancreatic cancers (more than 90%) contain a K-*ras* gene mutation at codon 12,[16,17] little is known about the expression or function of MSX2 as a candidate downstream gene of K-*ras* in pancreatic cancer. Therefore, we tested whether the presence of MSX2 would correlate with the malignant behavior of pancreatic cancer cells. Here we clearly show that MSX2-transfected pancreatic cancer cells demonstrate an enhanced malignant phenotype *in vitro* and *in vivo*, and that intense expression of this gene is frequently found in human pancreatic cancer tissues.

Materials and Methods

Cell Culture, RNA Extraction, and Reverse Transcription-Polymerase Chain Reaction (RT-PCR) for Cell Lines

Four pancreatic cancer cell lines (AsPC-1, BxPC3, Panc-1, and MIAPaca2) were purchased from American Type Culture Collection (Manassas, VA), routinely grown in modified Eagle's medium (Invitrogen, Grand Island, NY) containing 10% fetal bovine serum (Miles, Kankakee, IL) were maintained at 37°C in 5% CO_2 in a humidified environment.

Human pancreatic stellate cells were isolated from the surgically resected normal pancreas tissues of patients with pancreatic cancer, under the approval by the Ethics Committee of Tohoku University School of Medicine. The cells were maintained in Ham's F-12/Dulbecco's modified Eagle's medium containing 10% heat-inactivated fetal bovine serum (ICN Biomedicals, Aurora, OH), penicillin sodium, and streptomycin sulfate. Human umbilical vein endothelial cells and their optimized culture medium were purchased from Clonetics (San Diego, CA). Human umbilical vein endothelial cells were grown on 0.2% gelatin-coated tissue culture dishes (Corning, Corning, NY).

For cell RNA, total RNA was prepared using the RNeasy kit (QIAGEN, Hilden, Germany) with DNase treatment to eliminate DNA contamination according to the protocol provided by the manufacturer. First-strand cDNA was generated from 1 μg of total RNA using RETROscript (Ambion, Austin, TX) in a total volume of 20 μl according to the manufacturer's protocol. PCR was performed on 2 μl of RT product in a 25 μl of reaction mixture using Ex Taq polymerase (Takara, Ohtsu, Japan) with 3' and 5' primer concentration of 10 μmol/L each. Gene expression was normalized to respective glyceraldehyde-3-phosphate dehydrogenase (GAPDH) level. The PCR conditions for our cDNA templates were optimized to ensure replication is in the linear phase for each primer set used. To quantify the gene expression level, we also exploited quantitative real-time RT-PCR using LightCycler and LightCycler-FastStart DNA Master SYBR Green I (Roche Diagnostics, Basel, Switzerland). All reactions were performed according to the manufacturer's protocol. The annealing temperature for these primer sets was 60°C. The specificity of each PCR reaction was confirmed by melting curve analyses. The level of target gene expression in each sample was normalized to the respective GAPDH expression level. Each experiment was repeated at least three times, and representative data are shown. The primer pairs used were: MSX2, forward 5'-GGAGCGGCGTGGATGCAGGAA-3' and reverse 5'-AAGCACAGGTCTATGGAACGG-3', which span the approximately 3.5 kbp intron[18,19]; GAPDH, forward 5'-GGGAAGGTGAAGGTCGGAG-3' and reverse 5'-GAGGGGGCAGAGATGATGA-3'; and Twist 1, forward 5'-CACTGAAAGGAAAGGCATCA-3' and reverse 5'-GGCCAGTTTGATCCCAGTAT-3'.[20]

Generation of MSX2 Overexpressing Pancreatic Cancer Cell Lines

The PCR-amplified coding region of human MSX2 (808 bp, containing amino acids 1-267) using full-length human cDNA (provided by Dr. Takahashi, Kyoto University, Japan) as a template was subcloned into the pCDNA3.1 v5 vector (Invitrogen Life Technologies, Carlsbad, CA) in the sense orientation. Transfection of cells with expression vectors (MSX2 cDNA or vector alone) was performed using FuGENE 6 (Roche, Indianapolis, IN) as recommended by the supplier and cell lines were selected with 800 μg/ml G418 (Invitrogen). After G418 selection, clones were subjected to Western blot analyses with a specific antibody against v5 (Invitrogen) to confirm MSX2 expression. After establishment of empty vector (EV) or MSX2-transfected clonal cell lines, the same passages were used for each experiment.

RNA Interference

The small interfering RNA for MSX2 (MSX2 siRNA) expressing vector was generated by cloning the following annealed and *Bam*HI and *Hind*III digested oligonucleotides into pBAsi-U6 Neo DNA vector (Takara Bio Inc., Ohtu, Japan): 5'-GATCCACACAAGACCAATCGGAAGTTCAAGAGACTTCCGATTGGTCTTGTGTTTTTTTA-3' and 5'-AGCTTAAAAAAACACAAGACCAATCGGAAGTCTCTTGAACTTCCGATTGGTCTTGTGTG-3'. This generates siRNA directed against the sequence 5'-ACACAAGACCAATCGGAAG-3', corresponding to nucleotide human MSX2 at 409 to 428 (NCBI access number NM_002449) under the control of the human U6 promoter. The MSX2si expression vector or empty vector was transfected into Panc-1 cells using FuGENE 6 (Roche) as recommended by the supplier. After G418 selection, clones were subjected to RT-PCR to confirm MSX2 expression.

Western Blot Analysis

For whole-cell protein extraction, cells were lysed by the addition of lysis buffer (50 mmol/L Tris-Hcl, pH 7.4, 1% Nonidet P40, 0.5% sodium deoxycholate). Nuclear protein was extracted with nuclear and cytoplasmic extraction reagents (Pierce Biotechnology Inc., Rockford, IL) according to the manufacturer's recommendations. Cytosolic and membrane protein were extracted using a cell compartment kit (Qiagen) according to the manufacturer's protocol. Protein concentration in each sample was determined using the Bradford assay kit (Dojin, Kumamoto, Japan). After addition of 5X sample buffer (1 mol/L Tris-HCl, pH 6.8, sodium dodecyl sulfate, glycerol, and bromphenol blue) the aliquots were boiled for 5 minutes and subjected to 12.5% sodium dodecyl sulfate-polyacrylamide gel electrophoresis. After blocking for 1 hour at room temperature in a buffer containing 10 mmol/L Tris-HCl (pH 7.5), 100 mmol/L NaCl, 0.1% Tween 20, and 5% dry milk, nitrocellulose membranes (Bio-Rad Laboratories, Hercules, CA) were incubated either with monoclonal mouse v5 antibody (Invitrogen), monoclonal mouse monoclonal mouse β-catenin antibody (BD Transduction Laboratories, Lexington, KY), polyclonal rabbit Twist 1 antibody (Santa Cruz Biotechnology, Inc. Santa Cruz, CA), polyclonal lamin B1 antibody (Santa Cruz Biotechnology, Inc.), polyclonal GAPDH antibody (Trevigen, Gaithersburg, MD), polyclonal TIMM23 antibody (ProteinTech Group, Inc, Chicago, IL), or monoclonal mouse α-tubulin (Santa Cruz Biotechnology) antibody overnight at 4°C. The membranes were then washed with a buffer containing 10 mmol/L Tris-HCl, pH 7.5, 100 mmol/L NaCl, 0.1% Tween 20 and incubated with anti-goat (Zymed Laboratories, South San Francisco, CA), anti-rabbit, or mouse-IgG coupled to peroxidase (Amersham Biosciences, Buckinghamshire, UK) for 1 hour at room temperature. Reactive bands were detected using ECL chemiluminescence reagent (Amersham Biosciences). The obtained bands were subjected to densitometry analysis by using Scion Image Software (Scion Corporation, Frederick, MD).

Fluorescence Immunohistochemistry

MSX2- or EV-transfected BxPC3 cells and EV- or MSX2si-transfected Panc-1 cells were grown to subconfluence on BD Falcon culture slides (BD Biosciences, San Jose, CA) and fixed with ice-cold methanol (Wako, Osaka, Japan). After blocking with normal goat serum, cells were incubated with mouse monoclonal E-cadherin antibody (Santa Cruz Biotechnology) or monoclonal mouse β-catenin antibody (BD Transduction Laboratories) overnight at 4°C, and then slides were incubated with fluorescein-conjugated goat anti-mouse IgG (Jackson ImmunoResearch Laboratories, Inc., West Grove, CA). Cells were then incubated with propidium iodide (Wako) for nuclear staining and mounted with Vectashield (Vector Laboratories, Inc.). Cells were then incubated with propidium iodide (Wako) for nuclear staining and mounted with Vectashield (Vector Laboratories, Inc.). For double staining for MSX2 and Twist-1, cells were fixed with ice-cold methanol. After blocking with 3% bovine serum albumin in phosphate-buffered saline, cells were incubated with goat polyclonal anti-MSX2 antibody (Santa Cruz Biotechnology, Inc.) and rabbit polyclonal Twist-1 antibody (Santa Cruz Biotechnology, Inc.) overnight at 4°C, and then slides were incubated with Alexa Fluor 546 donkey anti-goat IgG (Molecular Probes, Eugene, OR) and Alexa Fluor 488 donkey anti-rabbit IgG (Molecular Probes), respectively, and mounted with Vectashield (Vector Laboratories, Inc). Cells were visualized for immunofluorescence with a confocal TIRF-C1 microscope (Nikon Instech Co., Ltd, Kawasaki, Japan).

Cell Growth Assays

For the cell growth assay, 6000 MSX2-transfected cells, MSX2 antisense-transfected cells, or EV cells were seeded per well in 96-well plates (Corning Incorporated, Corning, NY) in normal cell growth media. The 5-bromo-2-deoxyuridine assay was performed after 24 hours and 72 hours of incubation using a kit (Roche) according to the manufacturer's protocol. For each cell line the proliferation index was evaluated and the absorbance at 72 hours normalized to that at 24 hours.

Soft Agar Assay

For soft agar assay, 4×10^4 transfected BXPC3 cells were suspended in 0.3% Bacto agar (BD Falcon) supplemented with Dulbecco's modified Eagle's medium containing 10% fetal bovine serum and layered over 1 ml of an 0.8% agar medium base layer in six-well plates. After 21 days, the cells were stained with nitroblue tetrazolium (Roche), and anchorage-independent growth was estimated by counting the number of colonies using a microscope in high-power view.

Scrape Motility Assay

Pancreatic cancer cells were grown to confluence in 24-well culture dishes (BD Falcon) with normal growth media. The cell monolayer was mechanically scarred with a sterile pipette tip, and the plates were incubated with serum-free Dulbecco's modified Eagle's medium for an additional 2 to 4 days. Cells were visualized with an Olympus model CK2 inverted microscope using a 10X objective. Images were captured in a time-lapse manner with an Olympus C2000 digital camera. The scratched area covered by migrated cells was measured in three independent wells and normalized to initial scratched area using Scion Image Software (Scion Corporation).

Two-Chamber Migration Assays

Cell invasion was also determined by using a modified two-chamber migration assay (8-mm pore size, BD Biosciences) according to the manufacturer's instructions. A total of 1×10^4 cells were seeded in serum-free medium

in the upper chamber, and migration during 24 hours toward the lower chamber that contained 10% fetal bovine serum as a chemoattractant was evaluated. Cells in the upper chamber were carefully removed using a cotton bud, and cells at the bottom of the membrane were fixed and stained with Diff-Quick (International Reagents Corp., Kobe, Japan). Quantification was performed by directly counting in random 5 high-power fields after 24 hours of incubation.

Tumor Growth in Nude Mice

Tumor formation *in vivo* was assayed in female athymic nude mice by subcutaneously injecting each of 2×10^6 cells suspended in 200 μl of sterile phosphate-buffered saline. Tumor volume was measured every week after the first incidence of tumor formation. Volume was determined by the equation $V = L \times W^2 \times 0.5$, where V is volume, L is length, and W is width. The mice were sacrificed 7 weeks after injection and confirmed the histology confirmed by hematoxylin and eosin staining.

Orthotopic Implantation

To assess metastasis formation, MSX2-, MSX2si-, and empty vector-transfected pancreatic cancer cells (1.5×10^6 cells suspended in 50 μl) were injected into the pancreatic tails of female athymic nude mice. The mice were sacrificed 7 weeks after injection and tumor progression was confirmed. Histology was evaluated by hematoxylin and eosin staining.

Microarray

CodeLink Whole Human Genome Expression Bioarray (Amersham Biosciences), representing approximately 55,000 of the most well annotated human genes published in public databases, was used for cDNA microarray analysis. The platform employs single-color detection rather than a dual-color detection system, where multiple experiment comparisons are possible without replicating the reference sample. Procedures were performed according to the manufacturer's protocol, and all reagents were provided in the CodeLink Expression Assay Kit (Amersham Biosciences). In brief, 10-μg aliquots of total RNA was fragmented at 94°C for 20 minutes in the presence of magnesium. The fragmented RNA was hybridized to Uniset Human Whole Genome Expression Bioarray slides in hybridization buffer at 37°C for 24 hours in an INNOVA 4080 shaking incubator (New Brunswick Scientific, Edison, NJ) at 300 rpm. After hybridization, the arrays were washed in 0.75X TNT buffer [1X TNT: 0.1 mol/L Tris-HCl (pH 7.6), 0.15 mol/L NaCl, and 0.05% Tween 20] at 46°C for 1 hour followed by incubation with Cy5-streptavidin at room temperature for 30 minutes in the dark. Arrays were then washed in 1X TNT four times for 5 minutes each followed by a rinse in 0.1X standard saline citrate/0.05% Tween 20 in water. The slides were then dried by centrifugation and kept in the dark until scanning.

Gene Expression Data Analysis

Array slides were scanned using an Array WoRx (GE Healthcare Bio-Sciences Corp., Piscataway, NJ), and expression values were measured and manipulated subsequently by CodeLink Expression Analysis version 4.0 software (Amersham Biosciences). Each array contains a total of 55,776 spots, of which 54,840 are for human (nonbacterial) genes. Among the 54,840 gene expression values, low-intensity spots whose values were less than the detection threshold were all adjusted to the threshold. All good quality spots indicated by "G" flag as well as the low-intensity spots indicated by "L" were further processed for the statistical analysis. Those spots with poor quality were excluded from the analysis. Statistically, 54,530 spots were detected as either "G" or "L" flag in both experiments (B3-EV versus B7), thus most of genes are subsequently used in the following analysis.

To normalize data we compared the gene expression values from the two experiments and drew an intensity-ratio plot (MA plot). For each data point, an intensity (A) dependent normalization method (LOWESS)[21] is applied for adjusting the ratio (M) value. In LOWESS, we used the simple adjusting method that is $\log_2 M - c(A)$, where $c(A)$ is the mean ratio of the nearest 10,000 data points surrounding the current data point. After the calibration of M values, P values for evaluating how significantly those M values were apart from the mean were obtained under a cumulative normal distribution model whose variance is calculated with the same 10,000 data points. The array data were deposited in the National Center for Biotechnology Information Gene Expression Omnibus database (GSE6585).

Tissues, Immunohistochemistry, and Fluorescence Immunohistochemistry

Pancreatic cancer tissues were obtained from patients who underwent surgical operations for the tumors. The tissues collected at the time of surgery were immediately embedded in Tissue-Tek O.C.T. compound medium (Sakura, Tokyo, Japan), frozen in liquid nitrogen, and stored at −80°C or fixed in 10% paraformaldehyde overnight and embedded in paraffin wax. Thirty two pancreatic cancer tissues were used for the immunohistochemistry. The grade of differentiation and the stage of pancreatic cancer were determined according to methods described previously.[22,23] Informed consent was obtained from all patients before surgery.

Localization of MSX2 and Twist 1 in human pancreatic tissues was investigated by immunohistochemistry. The tissue sections were deparaffinized and antigens were retrieved by boiling the sections in Target Retrieval Solution (Dako, Carpinteria, CA) in the microwave oven. Then the sections were incubated in methanol with 0.3% hydrogen peroxide for 30 minutes to block the endogenous peroxidase activity. Thereafter, the Histofine kit (Nichirei, Tokyo, Japan) for MSX2 (Santa Cruz Biotechnology, Inc.) or the Santa Cruz staining kit for Twist 1 (Santa Cruz Biotechnology, Inc.) was used. Visualization of the immu-

noreaction was performed in 0.06 mmol/L 3,3'-diaminobenzidine tetrahydrochloride (Dojin, Kumamoto, Japan) containing 2 mmol/L hydrogen peroxide in phosphate-buffered saline for several minutes at room temperature. For the negative control, the immunostaining processes were performed by replacing the primary antibody with phosphate-buffered saline. The negative control sections showed no specific immunoreactivity. In addition, the specificity of antibody was determined in an absorption test using an excess amount of blocking peptide for MSX2 antibody (sc-17729 P, Santa Cruz Biotechnology, Inc.). Fluorescence immunohistochemistry was performed described above using 8-μm sections from the frozen tissues.

The degree of immunostaining for MSX2 was evaluated as follows: negative, less than 5% positive cells found; weak, 5 to 30% positive cells observed; moderate, 30 to 75% positive cells observed; intense, more than 75% immunoreactive cells observed in most areas of the tissue sections. The immunostaining for Twist 1 was judged positive when more than 10% of positive nuclear cells was observed. The evaluation of immunostaining was done independently by two observers (K.S. and A.K.) who had not been informed of the histological diagnosis.

Statistical Analysis

The computer software StatView for Macintosh (Abacus Concepts, Berkeley, CA) was used for all statistical analyses. The correlation of MSX2 expression with the patient's clinicopathological variables and the correlation between orthotopic injected mice and metastasis or dissemination were analyzed by the χ^2 test. The differences among the cells for proliferation and anchorage-independent growth were statistically analyzed by analysis of variance. The difference between two groups was statistically analyzed by unpaired *t*-test or Mann-Whitney *U*-test. A *P* value of <0.05 was regarded as statistically significant.

Results

Detection of MSX2 Expression in Pancreatic Cancer Cells

First, we examined MSX2 expression in pancreatic cancer cell lines and compared their expression level to pancreatic stellate cells or human umbilical vein endothelial cells. The quantitative real-time RT-PCR showed a difference in the MSX2 expression level of each cell line and revealed higher expression in carcinoma cells than in normal cultured cells (pancreatic stellate cells or human umbilical vein endothelial cells (Table 1). MSX2 expression was intense in Panc-1 and ASPC-1 cells, weak in MIAPaCa2, and very faint in BxPC-3 cells. Interestingly, the expression level of MSX2 was higher in K-*ras* gene-activated cell lines than in wild-type cell line BxPC3[24] (Table 1). The expression level of MSX2 in BxPC3 cells was similar to that of normal cultured cells, suggesting that this did not function as a carcinoma-related gene in this cell line. Therefore, we chose BxPC3 cells to confirm the effect of MSX2 in the gain-of-function manner.

Table 1. Relative Expression of MSX2 in Various Cell Lines and K-*ras* Mutation

Cell	Relative MSX2 expression	K-*ras* mutation[24]
Panc-1	1	+
AsPC-1	0.87	+
MIAPaca2	0.3	+
BxPC3	0.02	−
Pancreatic stellate cell	0.01	ND
Human umbilical vein endothelial cell	0.001	ND

ND, not done.

Generation of Stable Forced MSX2-Expressing and Inactivated Cell Lines and Morphology of These Cells

The MSX2- or MSX2si-transfected cells were cloned and subjected to Western blot analysis or quantitative real-time RT-PCR to confirm the expression of v5-tagged MSX2 protein or MSX2 RNA, respectively. We generated several clones of BxPC3 stably overexpressing MSX2 and Panc-1 stably expressing MSX2si; representative clones are shown in Figure 1. A significant morphological difference was observed between MSX2-transfected cells (B21 and B7) and control cells (parental BxPC3 and B3-EV). As shown in Figure 1B, B21 and B7 cells showed loose cell junctions and scattered morphology relative to control cells. The MSX2-expressing cell lines, B21 and B7, demonstrated a more fibroblast-like appearance compared to parental and B-3EV cells. This alteration of morphology resembled a mesenchymal phenotype rather than the usual phenotype of BxPC3, indicating that the cells were undergoing epithelial to mesenchymal transition (EMT) by MSX2 overexpression. A similar morphological change was observed between MSX2-expressing and down-regulated Panc-1 cells. As shown in Figure 1D, MSX2-expressing parental Panc-1 and EV cells showed loose cell junctions and scattered morphology, whereas the MSX2 down-regulated cell lines, si201 and si215, demonstrated a cobblestone-like phenotype.

To determine whether forced expression of MSX2 led to changes consistent with EMT, we examined immunofluorescence staining for epithelial markers such as E-cadherin and β-catenin on MSX2-expressing and down-regulated pancreatic cancer cells. As shown in Figure 2A, BxPC3 cells transfected with MSX2 exhibited weakly diffuse distribution of E-cadherin and β-catenin in the cytoplasm, whereas control cells (B3-EV) showed dominant membrane-bound staining. Consistently, Western blotting showed that the expression of E-cadherin was decreased and that nuclear and cytosolic expression of β-catenin was increased, whereas membranous β-catenin expression was reduced in MSX2-expressing cells (Figure 2, C and D). These molecular changes in MSX2-

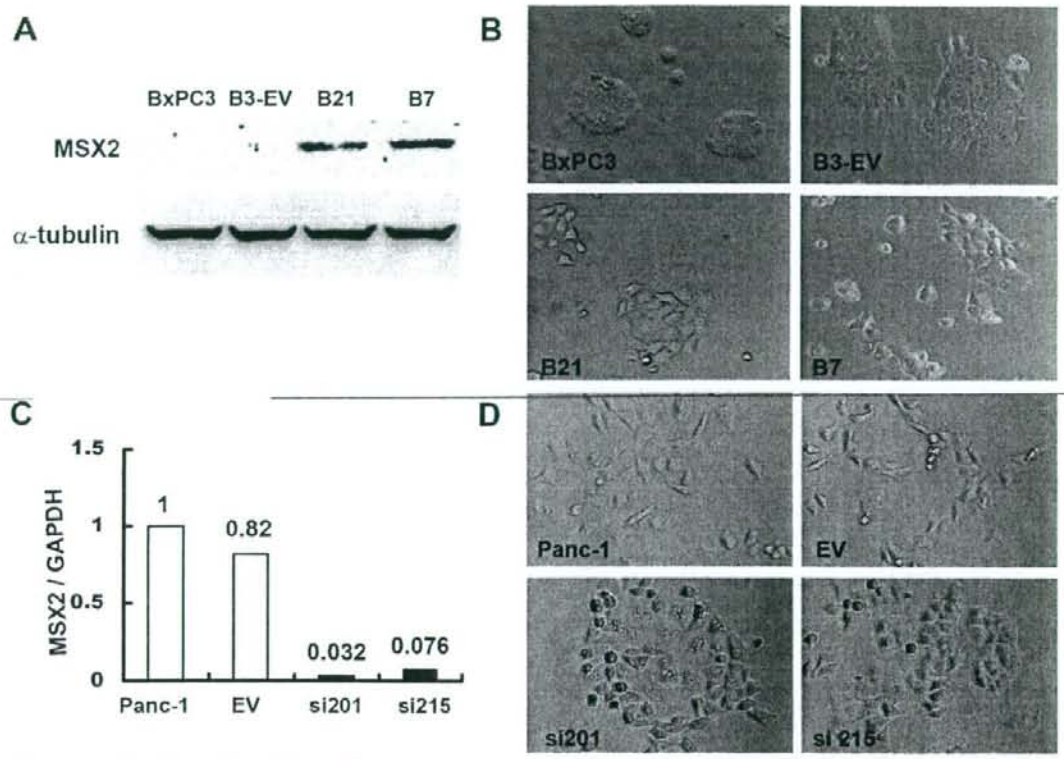

Figure 1. Morphological changes in MSX2- and MSX2si-transfected cells. **A:** Forced MSX2 protein expression is confirmed by v5 tag in B21 and B7 cells by Western blot using anti-v5 antibody. Stable MSX2-expressing cell clones were generated by G418 selection after transfection of MSX2 expression vector into BxPC3 whose MSX2 expression is lowest among the examined pancreatic cancer cell lines. **B:** Stable MSX2-expressing BxPC3 clones (B21 and B7) show loose cell contacts and have a fibroblast-like cell appearance relative to empty vector-transfected control cells (B-3EV) and parental BxPC3 cells. Original magnification, ×10. **C:** MSX2 inactivation is confirmed by quantitative real-time RT-PCR. This method clearly demonstrates the reduction of MSX2 expression in si201 and si215 cells compared to EV and parental Panc-1 cells. Expression of MSX2 mRNA was normalized to that of GAPDH mRNA. Values are expressed relative to 1.00 for expression in Panc-1 cells. **D:** Parental Panc-1 and EV-transfected cells show loose cell contacts and more fibroblast-like phenotype than MSX2 inactivated cells (si201 and si215). MSX2 down-regulated cells changed morphology to cobblestone-like appearance. Original magnification, ×10.

expressing cells are consistent with EMT. On the other hand, fluorescence immunostaining and Western blotting demonstrated that the membranous expression of E-cadherin and β-catenin was increased in MSX2si cells, whereas cytoplasmic or nuclear expression of these proteins was up-regulated in control cells (Figure 2, B–D).

MSX2 Promoted Growth Rate and Anchorage-Independent Cell Growth of Pancreatic Cancer Cells

To assess the effects of MSX2 on pancreatic cancer cell proliferation, a 5-bromo-2-deoxyuridine assay was used. B21 and B7 cells showed significant induction of proliferation after 72 hours of culture with normal medium compared to control cells (BxPC3 versus B7, $P = 0.032$; BxPC3 versus B21, $P = 0.032$; EV versus B7, $P = 0.003$; EV versus B21, $P = 0.006$) (Figure 3A). To elucidate the functions of MSX2 in anchorage-independent growth of pancreatic cancer cells, we used the soft agar assay. BXPC-3 cells overexpressing MSX2 showed a large number of colonies on soft agar, whereas parental and B-3EV cells showed very few colonies after 3 weeks of culture on soft agar (Figure 3B and Supplementary Figure S1A at *http://ajp.amjpathol.org*). Fourfold and sixfold more colonies were seen with B21 and B7 cells, respectively, compared to control cells ($P < 0.05$).

MSX2 Facilitated Cell Migration

We next examined the cell migration ability of MSX2-expressing and down-regulated pancreatic cancer cells by a wound-healing scratch assay and two-chamber migration assay. Because serum has been shown to activate mitogen-activated protein kinase,[25] the wound healing scratch assay was performed under serum-starved conditions. As shown in Supplementary Figure S1B (*http://ajp.amjpathol.org*) and Figure 3C, MSX2-expressing pancreatic cancer cells covered the scratched area

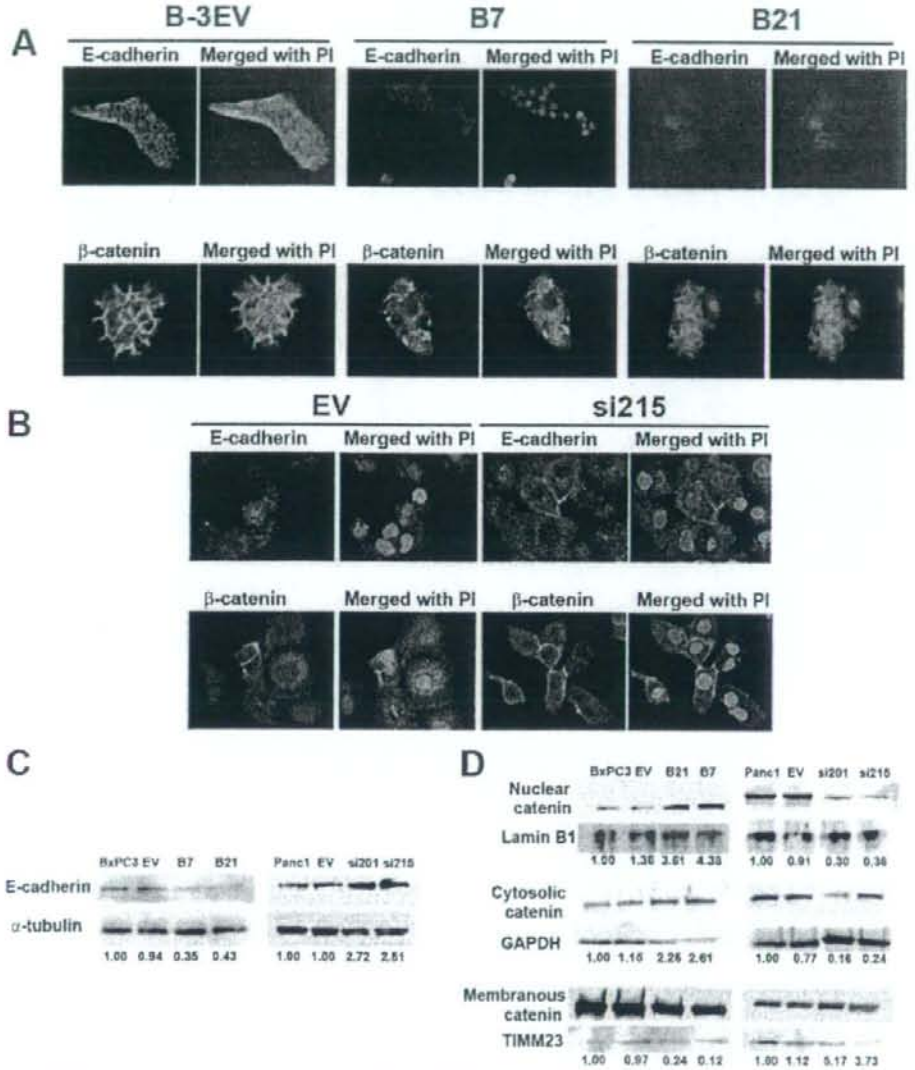

Figure 2. MSX2 induces morphological changes consistent with EMT in BxPC3 cells, and inactivation of MSX2 shows reverse effects on the state of EMT in Panc-1 cells. **A:** Immunofluorescence staining for E-cadherin and β-catenin was performed in empty vector- or MSX2-transfected cells. Dominant membranous expression of E-cadherin and β-catenin is seen in B-3EV cells, whereas these proteins are distributed within the cytoplasm and to a lesser extent within the nucleus in B7 and B21 cells. **B:** Immunofluorescence staining for E-cadherin and β-catenin was performed in empty vector- or MSX2si-transfected Panc-1 cells. Membranous expression of E-cadherin and β-catenin is lost and distributed within the cytoplasm and to a lesser extent within the nucleus in EV cells, while these proteins' localization is changed to the membrane in si215 cells, suggesting that reversal of EMT has occurred when MSX2 is down-regulated. **A** and **B**, original magnification ×20. **C:** To evaluate the expression level of E-cadherin, Western blots were performed, and the obtained bands were subjected to densitometry analysis. Expression of E-cadherin was normalized to that of α-tubulin protein. Values are expressed relative to 1.00 for expression in BxPC3 or Panc-1 cells. These analyses clearly revealed that E-cadherin expression was decreased in MSX2-expressing BxPC3 cells (B7 and B21) compared to control cells (BxPC3 and EV). On the other hand, MSX2 down-regulated Panc-1 cells (si201 and si215) showed restored expression of E-cadherin compared to control cells (Panc-1 and EV). **D:** Nuclear, cytosolic, and membranous protein was extracted and Western blots were performed to confirm the β-catenin expression level. The obtained bands were subjected to densitometry analysis and exhibited increased expression of nuclear and cytosolic β-catenin in B21 and B7 compared to control parental BxPC3 and B3-EV cells, while membranous expression was decreased in MSX2-expressing cells (B21 and B7). The Western blot also shows the reduced nuclear and cytosolic expression of β-catenin in MSX2si cells compared to EV and parental cells, whereas membranous expression was increased in MSX2si cells. Lamin B1, GAPDH, and TIMM23 were used as loading control for protein from nuclear, cytosolic, and membranous lysate, respectively. Expression of β-catenin was normalized to that of loading control. Values are expressed relative to 1.00 for expression in BxPC3 or Panc-1 cells. PI, propidium iodide.

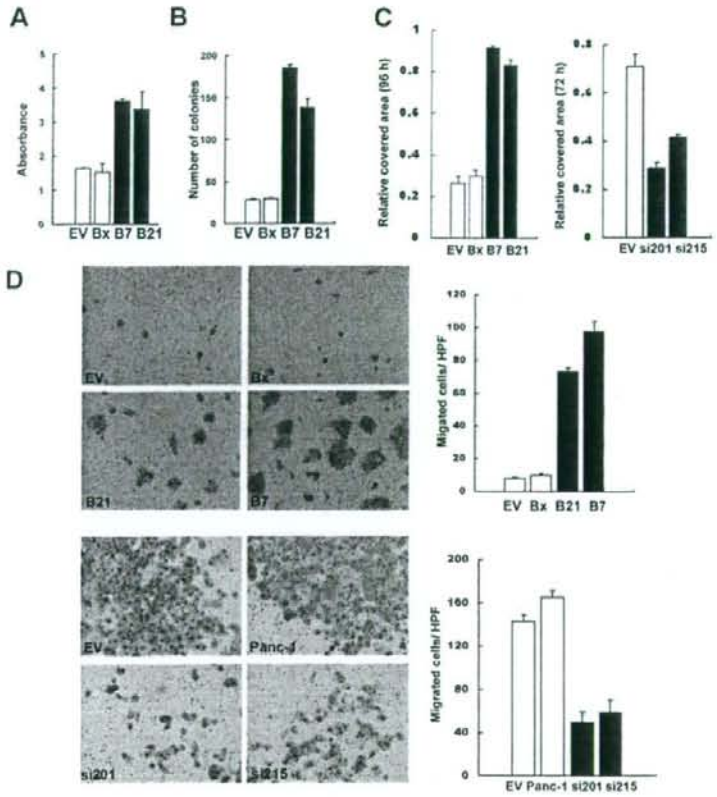

Figure 3. MSX2 enhances pancreatic cancer cell proliferation, colony formation on soft agar, and migration. The 5-bromo-2-deoxyuridine assay was used to examine cell proliferation after 72 hours of culture in normal growth medium. BxPC3 cells stably expressing MSX2 show a significant increase in cell proliferation. Statistical significance was observed between EV and B7 ($P = 0.003$), EV and B21 ($P = 0.006$), BxPC3 and B7 ($P = 0.014$), and BxPC3 and B21 ($P = 0.032$) (**A**). To determine the anchorage-independent growth of MSX2-expressing cells, we used soft agar assay. After 21 days of culture on soft agar, cells were stained with nitroblue tetrazolium and colonies were counted. Six- and fourfold more colonies are formed by B7 and B21 cells, respectively, compared to control parental and B-3EV cells. Statistical significance was seen between EV and B7 ($P = 0.003$), EV and B21 ($P = 0.006$), BxPC3 and B7 ($P = 0.014$), and BxPC3 and B21 ($P = 0.002$) (**B**). **C:** To assess cell migration, the wound healing scratch assay was performed. The scratched area covered by migrated cells was measured in three independent wells and normalized to the initial scratched area using Scion Image Software (Scion Corporation). MSX2-expressing cells show a larger number of migrated cells than control cells (C, left panel). In contrast, MSX2 down-regulated cells exhibit an inhibition of migration after 48 hours in serum-starved medium (**C**, right panel). **D:** Cell migration was further evaluated by two-chamber migration assay. Cells that migrated to the lower chamber were stained with Diff-Quick and directly counted. The photograph and bar graph clearly demonstrate the increased number of migrated cells in MSX2-expressing cells and fewer migrated cells in lower-expressing MSX2 cells.

with migrating cells in serum-starved conditions but B-3EV cells did not. The bar graph clearly shows that the number of migrated cells increased in a MSX2-dependent manner, indicating that MSX2 promoted cell migration (Figure 3C). In contrast, fewer MSX2 down-regulated cells (si201 and si215) migrated into the cell-free zone compared to the vector control cells (EV) (Figure 3C and Supplementary Figure S1C at *http://ajp.amjpathol.org*), indicating that down-regulation of MSX2 is associated with suppression of cell migration. To exclude the effect of proliferation to covered area in the scratch assay, we further examined the cell migration by the Transwell assay. As shown in Figure 3D, MSX2-expressing cells (B21 and B7 in upper panel, and EV and Panc-1 in lower panel) showed the large number of cells compared to MSX2 down-regulated (si201 and si215 in lower panel) or lower-expressing cells (EV and BxPC3 in upper panel).

MSX2 Promoted Cell Growth in Nude Mice

To determine whether MSX2 cells also promote tumor growth *in vivo*, 2×10^6 of EV cells or MSX2-expressing cells (B7) were injected subcutaneously into the dorsal flanks of nude mice. One week after injection, tumors began to appear in all B7-injected and some of the EV-injected nude mice. MSX2 derived tumors showed significantly faster growth and formed large tumors relative to those arising from EV cells (Figure 4A and Supplementary Figure S2A at *http://ajp.amjpathol.org*).

MSX2 Promoted Metastasis and Peritoneal Dissemination

To assess whether MSX2 expression also promotes cell migration or metastasis formation in an orthotopic environment, 1.5×10^6 EV cells, MSX2-expressing cells (B7), or MSX2si cells (si215) were injected into the pancreas of nude mice. Tumors were observed in the pancreas of mice implanted with all MSX2-expressing or MSX2si cells and control cells. MSX2-expressing cells frequently showed metastases to the liver (3/5, $P < 0.05$) and peritoneal dissemination (5/5, $P < 0.01$) while control cells demonstrated no liver metastasis or only one peritoneal invasion (Table 2 and Supplementary Figure S2, B–D, at *http://ajp.amjpathol.org*). In addition, histological examination revealed that MSX2 cells exhibited increased intercellular separation and loss of cell polarity (Figure 4B, d, f, and g) compared to those produced by EV cells (Figure 4B, b and e). On the other hand, the metastasis to the liver (0/5) and peritoneal dissemination were suppressed (0/5) in mice injected with MSX2 down-regulated

Table 2. Summary of Orthotopic Implantation of MSX2-Expressing or Inactivated Cells in Nude Mice

	N	Metastasis to liver	Dissemination to peritoneum
B-3EV	5	0	1
B7	5	3*	5**
EV (Panc-1)	5	4*	3*
MSX2si (Panc-1)	5	0	0

*$P < 0.005$; **$P < 0.01$; *$P < 0.005$ (χ^2 test).

cells, whereas mice implanted with control cells showed frequent liver metastasis (4/5, $P < 0.005$) and peritoneal dissemination (3/5, $P < 0.05$) (Table 2 and Supplementary Figure S2, E and F, at *http://ajp.amjpathol.org*). Tumors formed by control cells showed poorly differentiated fibroblast-like cells by histological examination (Figure 4C, left panel), while MSX2-inactivated cells formed mixed phenotype tumors where tubular type carcinoma cells were occasionally found (Figure 4C, right panel), indicating that MSX2 inactivation resulted in a reversal of the state of EMT.

MSX2 Up-Regulated Twist 1 Expression

To better understand the mechanisms underlying the effect of MSX2 in pancreatic carcinoma cells, we searched for differentially expressed genes in EV and B7 cells by cDNA microarray analysis. Among the genes significantly up-regulated by MSX2, we found Twist 1 as one of the most strongly induced genes in B7 compared to EV cells (Figure 5A). To confirm the result from the microarrays, RT-PCR and Western blotting were employed, using specific primers and antibody for Twist 1, respectively. As shown in Figure 5B, Twist 1 expression was induced in MSX2-expressing cells (B7 and B8, which expressed MSX2 weakly as shown in the upper panel in Figure 5B) compared to EV cells. In addition, the level of Twist 1 expression was consistent with that of MSX2. In addition, we examined double-fluorescence immunostaining to assess whether Twist 1 and MSX2 are coexpressed in pancreatic cancer cells. As shown in Figure 5C, MSX2-transfected BxPC3 showed simultaneous expression of these proteins in cancer cell nuclei; no coexpression was seen in empty vector-transfected BxPC3. Similarly, empty

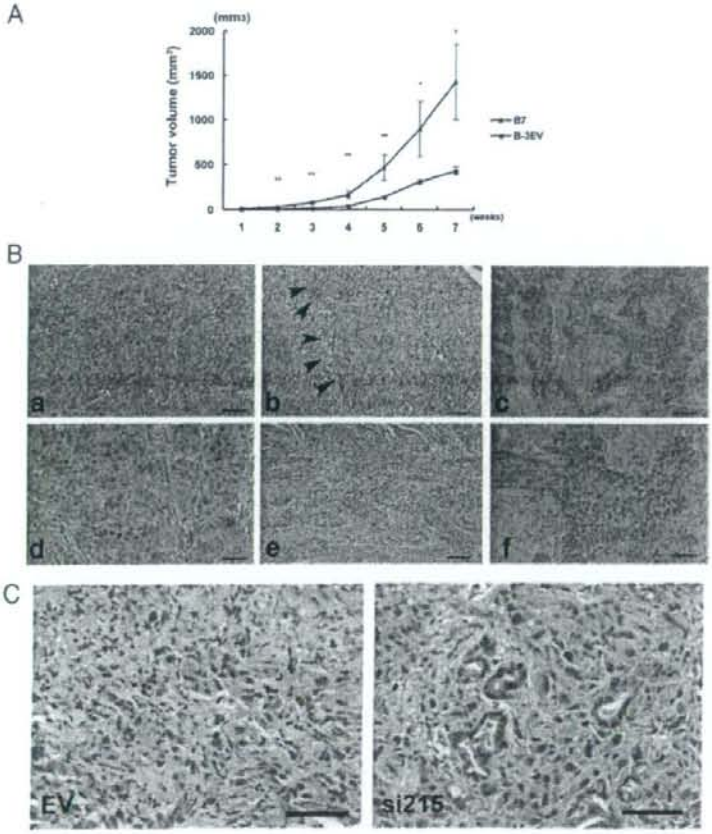

Figure 4. MSX2 enhanced tumorigenesis and metastasis in nude mice (**A–C**). Two million control (B3-EV) cells or MSX2-expressing (B7) cells were injected subcutaneously into the left and right sides of each mouse, respectively. After 7 weeks, mice were sacrificed, and B7 cells exhibited rapid growth as well as greater tumor size in nude mice relative to B-3EV cells. *$P < 0.05$; **$P < 0.01$ (**A**). Orthotopic implantation of MSX2-expressing cells shows significantly more evidences of the liver metastases and peritoneal dissemination (**B**). A total of 1.5×10^6 B3-EV and B7 cells were injected into the pancreatic tails of nude mice. Mice were sacrificed after 7 weeks, and development was examined. Control cells show small tumor without invasion to another site, while Msx2-expressing cells demonstrate liver metastases (**arrowhead** in **c**) or giant tumors invading the abdominal wall (**f**). Increased intercellular separation and loss of polarity are observed in tumors formed by B7 cells (**d**, **f**, and **g**) but not in tumors from B-3EV cells (**b** and **e**). **B**, **e** and **g**, are high-power views of **b** and **d**, respectively. Inactivation of MSX2 reduced metastasis and peritoneal dissemination of pancreatic carcinoma cells in orthotopic implantation in nude mice (**C**). EV and MSX2si cells were injected into the pancreas of nude mice to examine whether inactivation of MSX2 suppress pancreatic cancer development. Four of five and three of five control cells show metastasis to liver and dissemination to the peritoneum 7 weeks after orthotopic implantation, respectively. On the other hand, only a small tumor is observed in the pancreas of mice implanted with si215 cells. MSX2si-implanted mice did not show any metastasis to liver or dissemination or invasion into the abdominal wall. Histological examination revealed that control tumors show poor differentiation of the carcinoma cells (left panel in **C**), while tubular formation is occasionally seen in MSX2si tumors (right panel in **C**). Scale bar = 50 μm in **B** and **C**.

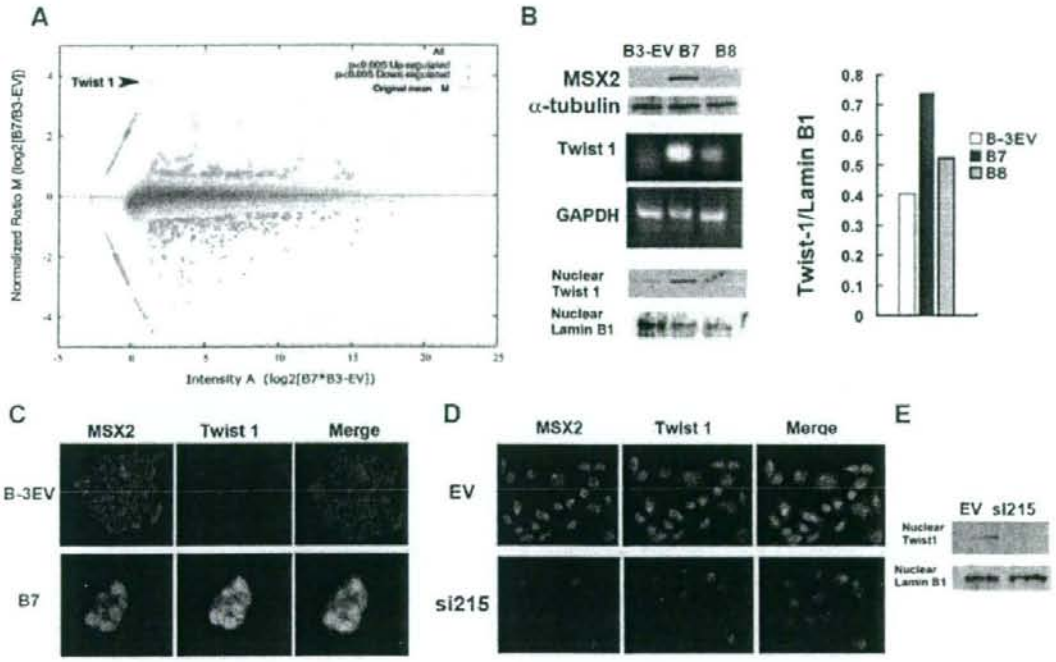

Figure 5. Microarray analysis reveals the induction of Twist 1 in MSX2-expressing cells. The plot shows M values (log2 B7/B3-EV ratio following LOWESS normalization) against A values (signal intensity flog2 B7*B3-EV]) for each spot in the microarray. Red circled plot and green asterisk plot represent genes whose expression was significantly ($P < 0.005$) up-regulated and down-regulated, respectively. This MA plot indicates that Twist 1 (**arrowhead**) is one of the most up-regulated genes in B7 compared to B3-EV cells (**A**). Twist 1 up-regulation in MSX2-expressing cells is confirmed by RT-PCR (middle panel in **B**) and Western blot (lower panel in **B**). The obtained bands were normalized to lamin B1 using Scion Image Software (Scion Corporation). This also indicates that the expression of Twist 1 is up-regulated in MSX2-expressing cells (bar graph in **B**). To examine the simultaneous expression of these proteins in pancreatic cancer cells, double immunofluorescence staining for MSX2 and Twist 1 was performed. MSX2-expressing cells (B7) show positive staining for Twist 1. The merge view demonstrates the yellow nuclear staining, indicating coexpression of MSX2 and Twist 1 in the nuclei (**C**). On the other hand, Twist 1 expression is not detected in cells with lower levels of MSX2 expression (B3-EV). Original magnification, ×20. **D:** Double immunofluorescence staining for MSX2 and Twist 1 was done to examine the synchronous of these proteins in pancreatic cancer cells. MSX2-expressing cells (EV) show positive staining for both MSX2 and Twist 1. The merge view demonstrates the yellow nuclear staining, indicating coexpression of MSX2 and Twist 1 in the nuclei (**D**). On the other hand, Twist 1 expression is not detected in cells with inactivated expression of MSX2 cells (MSX2si). Original magnification, ×20. **E:** Western blot analysis showed that nuclear expression of Twist 1 was found in EV cells but not in MSX2-inactivated cells (si215).

vector-transfected Panc-1 cells showed simultaneous expression of these proteins in cancer cell nuclei, but no coexpression was seen in MSX2 down-regulated Panc-1 cells (Figure 5D). Western blot also showed that nuclear Twist 1 expression was not detectable in MSX2si cells while clearly detectable in control cells (Figure 5E).

Expression of MSX2 and Twist 1 in Human Pancreatic Carcinoma Tissues

We next investigated MSX2 protein expression in human pancreatic cancer tissues by immunohistochemistry using a specific antibody and examined the association of its expression with clinicopathological features. Protein expression was found in cancer cell nuclei and occasionally in stromal cells neighboring the carcinoma cells (Figure 6A, a) while no or weak staining was seen in normal duct or acinar cells. Nuclear expression of MSX2 was found in 23 of 32 (71.8%) pancreatic cancer tissues. Among 32 cases of pancreatic carcinoma tissues, 10 cases (31.2%) were classified as intensely stained for MSX2, 8 cases (25%) were moderately stained, 5 cases (15.6%) were weakly stained, and 9 cases (28.1%) were negative for staining. Significant correlation was found between MSX2 expression and histological differentiation ($P = 0.004$) and vascular invasion ($P = 0.00003$) (Figure 6A and Table 3). However, there was no association of MSX2 expression with stage and T classification. The results of immunohistochemistry for MSX2 are summarized in Table 3.

Twist 1 expression was detected in nuclei and cytoplasm of cancer cells and in stromal cells near the carcinoma cells (Figure 6B, a and d). We evaluated its expression as positive when intense nuclear or cytoplasmic with nuclear staining was detected (Figure 6B, a and d), since weak cytoplasmic expression without nuclear staining was found in normal ducts. Positive Twist 1 expression was found in 14 of 32 (43.7%) cases of pancreatic cancer tissues. Double-fluorescence immunohistochemistry revealed that Twist 1 expression was observed in the carcinoma cells where MSX2 was expressed (Fig-

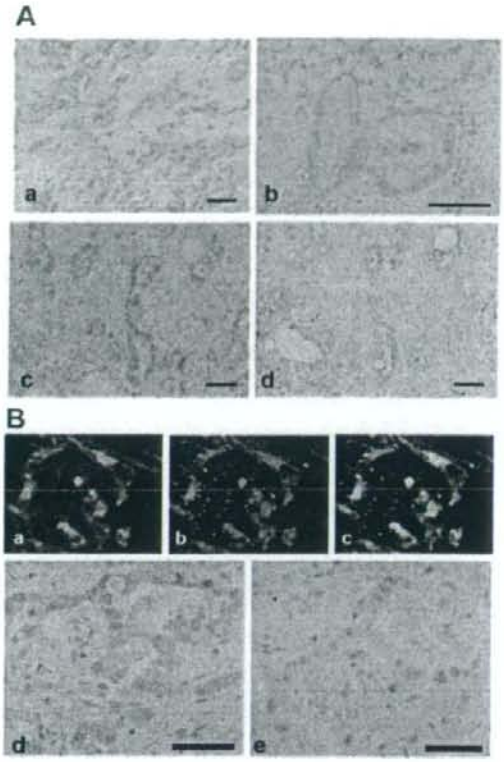

Figure 6. Expression of MSX2 and the association of its expression with Twist 1 in human pancreatic carcinoma tissues. **A:** MSX2 expression in human pancreatic carcinoma tissue was investigated by immunohistochemistry. Intense nuclear expression of MSX2 is detected in poorly (**a**) and moderately differentiated (**c**) pancreatic carcinoma cells, while no detectable level of MSX2 is present in well differentiated pancreatic carcinoma cells (**b**). **d:** The absorption test using an excess amount of blocking peptide for MSX2 antibody was performed in the serial section corresponding to **c**. No nuclear staining was found in the section. Scale bar = 50 μm. **B:** Correlation of these proteins was confirmed by double immunofluorescence staining (**a–c**) for MSX2 and Twist 1 or immunostaining (**d** and **e**) in serial human pancreatic cancer tissues. The expression of Twist 1 (**a**) and MSX2 (**b**) was observed in nuclei or in cytoplasm of pancreatic cancer cells. Original magnification, ×20. The yellow nuclear staining indicates coexpression of MSX2 and Twist 1 in cancer cell nuclei (**c**). Original magnification, ×20. Immunohistochemistry also showed nuclear expression of Twist 1 (**d**) in the serial section of moderate to poorly differentiated pancreatic carcinoma cells expressing MSX2 (**e**). Scale bar = 50 μm in **d** and **e**.

ure 6B, a–c) and was significantly associated with increased expression of MSX2 ($P = 0.0009$, Table 4).

Discussion

EMT is characterized by disassembly of cell-cell contacts, reorganization of the actin cytoskeleton, and cell-cell separation brought on by β-catenin relocalization. Together these events result in fibroblast-like cells with mesenchymal marker expression and migratory properties during embryogenesis.[26,27] This transition is considered to be an important event during malignant tumor progression and metastasis.[28,29] On the other hand,

Table 3. Correlation between Clinicopathologic Findings and MSX2 Expression

	MSX2 staining		
	<30%	>30%	*P* value*
Age			0.96
<60	4	5	
>60	10	13	
Gender			0.34
Male	7	12	
Female	7	6	
Stage			0.957
I	1	2	
II	1	1	
III	4	4	
IV	8	11	
T classification			0.971
T1	1	2	
T2	3	3	
T3	6	8	
T4	4	5	
Lymph node metastasis			0.41
Negative	2	6	
Positive	12	12	
Histological classification			0.00436
Well	8	2	
Moderately	6	9	
Poorly	0	7	
Lymphatic invasion			0.365
Ly0	2	5	
Ly1	7	5	
Ly2	4	7	
Ly3	1	0	
Vascular invasion			0.00003
v0	0	3	
v1	6	1	
v2	8	1	
v3	0	12	
Perineutral invasion			0.257
n0	1	5	
n1	5	2	
n2	3	3	
n3	5	7	

*Analyzed by χ^2 test.

β-catenin/LEF-1 signaling has been shown to be up-regulated during EMT in mammary epithelial cells stably expressing c-Fos.[30] Induction of EMT by this signaling pathway was also reported in other epithelial cell lines,[31,32] indicating that the β-catenin pathway plays a crucial role in EMT. Thus the reports that induction of MSX2 by β-catenin/LEF-1 signaling[33] and that MSX2-transduced mesenchymal 10T1/2 cells exhibited increased nuclear β-catenin localization[34] raised the question of whether or not MSX2 itself could lead the epithelial

Table 4. Correlation between Nuclear Expression of Twist 1 and MSX2

	Twist 1		
	10% > nuclear staining	10% < nuclear staining	*P* value*
MSX2 expression			0.0009
<30%	13	1	
>30%	5	13	

*Analyzed by χ^2 test.